CLIMATE EXTREMES IN THE NEW ZEALAND REGION: MECHANISMS, IMPACTS, ATTRIBUTION

M James Salinger[1], Kevin E Trenberth[2,3], Howard J Diamond[4], Erik Behrens[5], B Blair Fitzharris[6], Nicholas Herold[7], Robert O Smith[8], Phil J Sutton[5] and Michael C T Trought[9]

[1]Department of Geography, Environment & Earth Sciences, Victoria University of Wellington, Wellington New Zealand

[2]Department of Physics, University of Auckland, New Zealand

[3]National Center of Atmospheric Research, Boulder, Colorado, USA/ Dept. Physics, University of Auckland, New Zealand

[4]NOAA/Air Resources Laboratory, College Park, Maryland 20740, USA

[5]National Institute of Water and Atmospheric Research, Wellington, New Zealand

[6]Department of Geography, University of Otago, Dunedin, New Zealand

[7]Applied Climate Science Pty Ltd., Adelaide, Australia

[8]Department of Marine Science, University of Otago, Dunedin, New Zealand

[9]Innovative Winegrowing, Blenheim, New Zealand

* Corresponding author: M. James Salinger, jimbosalinger09@gmail.com,

+ 64 21 221 9461

ORCID: 0000-0002-5782-1411

Abstract

As global surface temperatures have increased with human-induced climate change, notable compound climate extremes in the New Zealand (NZ) region associated with Atmospheric Heatwaves (AHW) and Marine Heatwaves (MHW) have occurred in the past six years. Natural modes of variability that also played a key role regionally include the Interdecadal Pacific Oscillation (IPO), El Niño/Southern Oscillation (ENSO), and changes in the location and strength of the westerlies as seen in the Southern Annular Mode (SAM). Along with mean warming of 0.8°C since 1900, a negative phase of the IPO, La Niña phase of ENSO and a strongly positive SAM contributed to five compound warm extremes in the extended austral summer seasons (NDJFM) of 1934/35, 2017/18, 2018/19, 2021/22 and 2022/23. These are the most intense coupled ocean/atmosphere (MHW/AHW) heatwaves on record with average temperature anomalies over land and sea +0.8 to 1.1°C above 1991- 2020 averages. The number of days above 25°C and above the 90th percentile of maximum temperature has increased, whilst the number of nights below 0°C and below the 10th percentile have decreased. Coastal waters around NZ recently experienced their longest MHW in the satellite era (1982-present) of 289 days through 2023. The estimated recurrence interval reduces from 1 in 300-years for the AHW event during the 1930s climate to a 1 in 25-year event for the most recent decade. Consequences include major loss of ice of almost one third volume from Southern Alps glaciers from 2017 to 2021 with rapid melt of seasonal snow in all four cases. Above average temperatures in the December/January grape flowering period resulted in advances in veraison (the onset of ripening); and higher-than-average grape yields in 2022 and 2023 vintages. Marine impacts include widespread sea-sponge bleaching around northern and southern NZ.

Keywords: Anthropogenic global warming, compound extremes, marine heatwave, atmospheric heatwave, extremes, impacts, terrestrial ecosystems, marine ecosystems, viticulture.

1. Introduction

The New Zealand (NZ) region, including its exclusive economic zone (EEZ) and extended continental shelf (ECS) from 25 to 56°S, 162°E to 171°W (see Figs.1 and 2), of 4.2 million km^2, is situated in the midlatitudes and experiences tropical and subtropical influences from the Pacific as well as high-latitude effects from the South Pacific and Southern Ocean. The oceanic circulation has been described by Chiswell et al. (2015) and Graham and De Boer (2013). Tropical convection in the equatorial Pacific has impacts on the large-scale Southern Hemisphere atmospheric circulation and therefore NZ climate through teleconnections, especially during extreme years of the El Niño Southern Oscillation (ENSO) (Kidson and Renwick 2002). Further, the strength and position of the subtropical jet, the subtropical high-pressure belt, and the subpolar westerlies influence NZ's climate (Clare et al. 2002), along with extratropical storm tracks (Simmonds and Keay 2000; Keable et al. 2002).

The Southern Annular Mode (SAM) is a hemispheric variation in the prevailing latitude of the main belt of zonal westerly winds and the associated jet streams and storm tracks. Here the term "storm tracks" refers to the tracks of cyclonic and anticyclonic perturbations and associated weather systems (Trenberth 1991). In the positive phase, the westerlies and storm tracks shift southwards and strengthen, with weaker westerlies and more settled conditions farther north. The SAM shows a general increase beginning in the 1960s consistent with a strengthening of the circumpolar vortex and westerlies that has been associated with the development of the ozone hole, especially in the southern summer, and greenhouse gas increases (Arblaster et al. 2011). Only in spring 2016 did the SAM turn abruptly negative in association with large decreases in Antarctic sea ice in all sectors. Despite a very strong negative SAM occurred in November 2016, the overall high values of SAM have continued.

The Inter-decadal Pacific Oscillation (IPO), and closely related Pacific Decadal Oscillation (PDO) pattern of sea surface temperatures (SST) is somewhat like that associated with ENSO, except

that, by design, it is focused in the extratropics (Trenberth et al. 1998). They have been described as a long-lived El Niño-like pattern of Indo-Pacific climate variability or as a low-frequency residual of ENSO variability on multi-decadal time scales. ENSO teleconnections on interannual time scales around the Pacific basin are significantly modified by the PDO/IPO (Trenberth et al. 2007).

El Niño, the warm ocean component of ENSO, refers to an anomalous warming of the surface tropical Pacific Ocean east of the dateline to the South American coast. The Southern Oscillation is the atmospheric component of ENSO and corresponds to a global-scale pattern in mean sea level pressure, and hence surface winds. The oceanic and atmospheric conditions in the tropical Pacific fluctuate somewhat irregularly between El Niño and the cold phase of ENSO: a basin-wide cooling of the tropical Pacific, named 'La Niña'. During La Niña the South Pacific High is stronger than normal and the South Pacific Convergence Zone (SPCZ) is farther southwest and closer to NZ, while lower pressures and wetter conditions tend to prevail over northern Australia. This often sets the stage for higher-than-normal pressures east or southeast of NZ and prevailing winds often have a northerly component.

Gregory et al. (2023) conclude that atmospherically driven marine heatwaves (MHW) in the Tasman Sea region are more likely to occur during the positive phase of SAM as part of an atmospheric zonal wave-3 pattern and is more likely to occur during La Niña years. These SAM events are linked to low wind speeds and increased downward solar radiation in the Tasman Sea, which lead to increased surface ocean temperatures especially through the reduction of mixing. Gregory et al (2024) suggest that the positive SAM phase presents a higher-than-average marine heatwave (MHW) hazard in most seasons. However, the positive phase of SAM has the strongest correlation in this region during spring when there is a higher likelihood of positive SAM events (Silvestri and Vera 2009).

The air temperature extremes each year can be compared to the estimated distribution of temperatures for the period before that occurrence. Trends in air temperature over land are greater

than those of surrounding SSTs (Mullan et al. 2010), although the increase in global and Southern Ocean heat content and SSTs has been significant recently (Cheng et al. 2024). Salinger et al. (2020) found the pattern of warming in NZ to be consistent with changes in SST and prevailing winds. Enhanced rates of warming along the East Australian coast and to the east of the North Island, and much lower rates of warming south and east of the South Island were shown in earlier work.

An ocean seasonal cycle is clearly evident in the upper 100–150 m (Pan et al. 2023). There is a marked warming signal through the late 1990s that extends through the full 800 m of the measurements (effectively the full depth of the eastern Tasman Sea, Fig. 1). It also began during the 1997/98 El Niño period when conditions would be expected to be relatively cool, thought to be linked to a large-scale warming event centred on 40° S that had hemispheric and perhaps global implications (Sutton et al. 2005, Bowen et al. 2006; Roemmich et al. 2007). The speeding up of the entire South Pacific gyre continued through to at least 2015 (Roemmich et al. 2016).

Compound climate extremes (Zscheischler et al. 2018) occur when (1) two or more extreme events occur simultaneously or successively, (2) combinations of extreme events with underlying conditions amplify the impact of the events, or (3) combinations of events that are not themselves extremes that lead to an extreme event and cascade down to impacts when combined. In the NZ oceanic locale, heatwaves driven by coupling of atmospheric and marine conditions making these events AHW/MHW.

The key aim of this paper is to provide a broad analysis of how Anthropogenic Greenhouse Warming (AGW) and each of these climate modes (IPO, ENSO, SAM) influence surface air and SST variability and the occurrences of AHW and MHW in the Tasman Sea/NZ region. We also consider the relative importance of compound drivers and their combined influence on temperature variability. This paper focusses on the most intense AHW and associated MHW for this region covering the austral warm seasons (November - March). We examine the effects of how compound extremes relate to the changing frequency of high and low temperatures, and the mechanisms

involved. Finally, we consider some consequences and impacts on marine and terrestrial ecosystems, including rapid loss of glacial ice, viticulture and near coastal marine biota. There is also an assessment of future likelihood of similar events.

2. Methods

2.1 Atmosphere and Oceans

SSTs were extracted for the NZ region of 4.2 million square kilometres and applied to identify and characterize MHW based on daily (i) area-averaged, and (ii) EEZ grid cells for both the NZ EEZ (NZEEZT), corresponding to an area 200 nautical miles in width seaward of the coastline, and Extended Continental Shelf (ECS) areas (NZEEZT) (Fig.2). Daily SST estimates came from the NOAA daily Optimum Interpolation SST version 2.1 analysis (OISSTv2.1) (Huang et al., 2020) on a 0.25° latitude/longitude grid spanning September 1981-July 2022. Monthly SST observations were obtained from ERSST version 5.2 (Huang *et al* 2017) on a 2° × 2° latitude/longitude grid from 1854.

Hobday *et al.* (2016; 2018) definitions were applied to identify MHWs based on daily SST measurements. This is when mean SST exceed the 90th percentile for at least 5 consecutive days, and with well-defined start and end times. Daily climatological mean and 90th percentile values were calculated over a 30-year baseline period (1991–2020) for each day of the year using all SST data within an 11-day window. The time series were smoothed with a 31-day moving window. The warming during each MHW was characterized using metrics (Fig. 4): duration (continuous period that SSTs exceed the 90th percentile value), maximum and mean intensity (the maximum and mean daily SST anomaly during each MHW).

The heatwave frequency (HWF) is defined as the number of heatwave days in a warm season (NDJFM) (Alexander and Herold, 2015). Heatwave days are defined using the Excess Heat Factor (EHF) as described in Perkins and Alexander (2013). The EHF takes into consideration both the

144 warmth of a day relative to the 1991-2020 climatological base period as well as relative to the
145 previous 30 days, to account for acclimatisation. A heatwave only occurs when the EHF is positive
146 for three or more consecutive days.

147 The 22-station NZ air temperature (NZ22T) series (Salinger et al. 1992; 2020) were used to
148 calculate monthly mean air temperature anomalies for 1934-2023, relative to the 1991-2020 normal.
149 Climpact software (Alexander and Herold 2015), was used to analyse daily climate extremes. Only
150 data from Wellington, Hokitika, Milford Sound, Mt Cook, Lincoln, Queenstown and Lauder were
151 available for analysis of the 1934/35 event, but at least 20 stations were included from 1951.

152 TX90p, TN10p (percentage of days when TX is above the 90th percentile and TN below the
153 10^{th} percentile), and number of days $\geq 25°C$ and $\leq 0ºC$, the latter for the calendar year, were
154 calculated and averaged over NZ during 1940-June 2023.

155 Atmospheric circulation is mainly based on monthly mean sea level pressures (MSLP)
156 anomalies for NDJFM with a 1991-2020 base period, and these were computed using the ERA5
157 reanalysis (Bell et al. 2021). 500-hPa geopotential heights for NDJFM could only be analyzed for the
158 four more recent seasons. Several indices used to characterize the anomalous circulation (Trenberth
159 1976; Kidson 2000) include Z1, which measures west-east (zonal) flow, and M1 which measures the
160 south-north (meridional) flow in the NZ region. Negative Z1 is typical in blocking situations when
161 the prevailing westerly to south-westerly flow is absent in the region, especially with negative M1
162 (northerly flow anomaly).

163 Subsurface temperatures for the eastern Tasman Sea (160–172°E, 35–45°S) were also
164 calculated using all available Argo (floats that measure temperature and salinity in the top 2000m of
165 the oceans) data (47–66 profiles per month, Jayne et al 2017). Temperature anomalies were
166 calculated by differencing the Argo profiles and co-located temperature profiles from the CSIRO
167 Atlas of Regional Seas (CARS) 2009 climatology (Ridgway et al 2002, based on all available data in
168 the region prior to 2009). The eastern Tasman region was chosen because it was an area of strong

SST change during this event and is oceanographically uniform by excluding strong gradients and variability associated with the Subtropical Front to the south, the Tasman Front to the north and the East Australian Current (EAC) to the west. The Argo minus CARS vertical temperature anomalies were regionally averaged, given the uniformity of the region and monthly averaged to increase the signal to noise.

The global ocean model hindcast analysed here is based on the ocean sea-ice component of the UK Earth System Model (Storkey et al 2018) and the New Zealand Earth System Model (NZESM; Williams et al 2016) using 1° × 1° tripolar model grid (eORCA1) to simulate the ocean and 75 vertical z-levels. Ocean physics have been simulated with the Nucleus for European Modelling of the Ocean (NEMO, Madec 2008) model using the recent released (3.6. stable) code version. Sea-ice has been modelled, using the Community Ice CodE (CICE, Hunke et al 2017). Atmospheric boundary conditions to force this ocean-only configuration are based on the atmospheric reanalysis product JRA-55-DO v1.3 (Tsujino et al 2018) and the ocean hindcast covers the period from 1958 until February 2018. The fully coupled version of this model (HadGEM3-GC3.1) has been shown to perform well against key metrics in a pre-industrial model setup (Menary et al 2018).

To also quantify oceanic changes around NZ we use the ORAS5 reanalysis product (Zuo et al. 2019). This global model data assimilation product provides physical ocean properties as monthly means from 1958 to present on a global 0.25° horizontal grid with 75 vertical z-levels. For this study we use potential temperatures and ocean heat content to characterize past anomalies relative to a 30-year long climatology (1991-2020) for November through March, centred around the Southern Hemisphere summer season. We evaluate ocean temperatures for the top 50m to capture and characterize the near-surface warming to complement the SST-anomalies obtained from satellite and in situ data. In addition, we use the top 300m heat content anomalies to provide a more complete picture how near-surface waters are warming around NZ.

194 A generalized extreme value distribution was fitted to the annual air temperature anomalies
195 from the 66-year period 1871-1935 for the 1934/35 extreme, and the 66-year period 1957-2022 for
196 the four more recent events. Expected probability of occurrence and the estimated return interval
197 (ERI) of the temperatures were made based on the two distributions for a warming scenario of 2°C.
198 The fifty years 1871-1920 is considered close to the "preindustrial" temperature distribution. This
199 was achieved by fitting generalized extreme value distributions to the observed temperature record
200 for 1871-1920, plus the relevant warming offset. This may capture the full distribution of
201 temperature expected in future better than obtained by using climate model estimates.

202 *2.2 Cryosphere and other consequences*

203 The end of summer snowline (EOSS) time series (Chinn et al. 2012) was used to estimate
204 Southern Alps glacier mass balance and ice volume in water equivalents from 1977 to 2021 for
205 $EOSS_{Alps}$. As these EOSS results are not necessarily robust (Dowson et al. 2020; Lorrey et al 2022)
206 $EOSS_{Alps}$, normalized data were obtained from the latest report (Willsman and Macara 2023). Two
207 methods are employed to monitor volume changes. Method 1 to monitor volume changes deals with
208 the rapid to normal response time glaciers, small to medium in size. It uses mass balance gradients
209 and glacier areas to convert changes in snowlines to changes in ice volume water equivalent. Ice
210 volume changes for 1976–2021 are calculated for each index glacier, and then extrapolated to most
211 other glaciers of the Southern Alps. Method II deals with 12 protracted response glaciers, which tend
212 to be large. Mass balance deficits and ablation from the 12 large, protracted response glaciers are
213 estimated using a geodetic approach based on topographic and lake changes determined from
214 repeated surveys.

215 Estimates of water stored as seasonal snow in the South Island for 2017/18, 2018/19, 2021/22
216 and 2022/23 were provided by the model "SnowSim" available through Meridian Energy Ltd
217 https://www.meridianenergy.co.nz/who-we-are/our-power-stations/snow-storage/ (Fitzharris and

Garr, 1996). SnowSim calculates water stored as seasonal snow for key hydrogenerating river catchments and is tuned to the long-term water balance.

Regional Marlborough yields of grapes and areas were sourced from annual NZ Winegrowers Vintage survey and Vineyard reports respectively. For *marine ecosystems,* the tissue necrosis of sponges was examined (Bell et al. 2022, 2024). The presence and severity of tissue necrosis affecting the massive sponges *Ecionemia alata* and *Stelletta conulosa* were made using existing photographic datasets, videos and in-situ observations at 1 - 20 m depth throughout northeastern NZ. Data were collected between February and July 2022. The presence and condition of other sponge species were also noted but not quantified. *Ecionemia alata* and *Stelletta conulosa* were assessed as either healthy, partially sick (<20% visible necrosis) or sick (>20% visible necrosis) (Marlow et al. 2018).

3. Results

3.1 Atmosphere and ocean temperatures

For the five most intense heatwaves, both land air and sea temperatures combined were 0.7° to 1.1°C above the NDJFM 1991-2020 averages over the entire region (latitude 32° to 52°S, and longitude 150°E to 180°) (Table 1 and Fig. 3). NZ22T anomalies (Table 1) ranged between 0.9°C and 1.6°C respectively (Fig. 3 a – e, and Table 1). The general pattern for the MHWs was one of highest anomalies to the west of the South Island of NZ, often extending east of the South Island to the 180° meridian, with anomalies as much as 1.5°C. The area affected was elliptical in shape extending from Bass Strait to east of 180°. The most extreme years were 2017/18 and 2022/23.

The four most intense coastal MHW (Fig. 4 and Fig.4e) in the satellite-era (1981-present) all occurred since 2017, during the austral summers 2017/18, 2018/19, 2021/22 and 2022/23. The most intense coastal MHW occurred during summer 2017/18, when the area-average SST for NZ waters were in a MHW state for 138 days with a maximum (mean) MHW intensity of 2.9°C (1.7°C). In

241 contrast, the longest lasting coastal MHW commenced during summer 2022/23 and persisted for 289
242 days, with a maximum (mean) intensity of 2.1°C (1.2°C).

243 The Argo measurements (Fig. 5) averaged over the eastern Tasman Sea showed a strong
244 surface-intensified anomaly between November 2017 and February 2018, peaking as a 3°C mean
245 anomaly in the upper 20m with positive anomalies extending to ~50m depth as the warm surface waters
246 were mixed down through the water column. There was a second warm anomaly between November
247 2018 and February 2019, this signal peaking at 2ºC in the upper 30m and extending down to 60m.
248 During these 2017/18 and 2018/19 events, warm anomalies extended down to 300 m east of the South
249 Island (not shown). Weaker warm anomalies with ~ 1ºC peaks occurred in 2021/22 and 2022/23.

250 *3.2 Climate indices*

251 For the five AHW days experiencing at least 25ºC over NZ averaged between 20 to 30 days
252 per event. TX90p was approximately 15-17%, an anomaly of +5-7% relative to the 1991-2020 base
253 period (Fig.6). Days below 0ºC halved, from 40 to 20 days per annum, mainly owing to
254 Antrhopogenic Global Warming (AWG) and the TN10p reduced from 16 to 8%, and around 6%
255 during the heatwave years. Although the warm (more) and cold (less) extremes stand out for the
256 individual heatwaves years there are clear positive trends for summer days/TX90p, and negative
257 trends in frost days/TN10p for the four recent years. Preliminary analysis of 5-day annual maximum
258 rainfalls did not yield conclusive results and will be the subject of further investigation.

259 HWF (Fig. 7), reveals that 2017/18 had the most heatwave days (35) followed by 1934/35 (27).
260 Next came 2021/22 with 21, and 2018/19 and 2022/23 with 15-16. 1998/99 recorded 17 heatwave
261 days. The 1934/35 season was most unusual given that the overall climate was at least 0.7ºC cooler.

262 *3.3 Atmosphere and ocean circulation*

263 The five NDJFM seasons (Fig. 8a, 8c, 8e, and 8g) and Kidson (1935) for 1934/35 show a
264 pattern of strong blocking (persistent higher than normal pressures) to the southeast of NZ often with
265 negative pressure anomalies northwest of NZ, and this was also true in 1934/35 (not shown). The M1

and Z1 circulation indices (Table 1) showed northeasterly airflow for four events, while 2021/22 is easterly. Kidson (2000) weather regimes showed a lack of zonal regimes throughout except for 2018/19, more blocking throughout 2017/18 and 2021/22, and negligible troughing in 2021/22.

The 500-hPa geopotential height anomalies were consistent (Fig. 8b, 8d, 8f, and 8h) with very strong blocking to the southeast of NZ. The 2017/18, 2021/22 and 2022/23 anomalies were the most intense, reaching 70 geopotential metres (gpm) or more to the southeast of the South Island.

In all five heatwave warm seasons the SAM was strongly positive (Table 1). The Niño 3.4 Index had weak values in 1934/35 (+0.1) but stronger in 2018/19 (+0.79). The 2017/18, 2021/22 and 2022/23 events were in the La Niña phase (-0.90, -0.97 and -0.56 respectively), and with the IPO strongly negative with positive values of the Southern Oscillation Index (SOI) values except for 2018/19 (Table 1).

3.4 Ocean reanalysis

All four selected summers are characterized by positive temperature anomalies over the top 50m around NZ (Fig. 9) relative to the 1991-2023 period. The spatial patterns for 2017/18 and 2018/19 are very similar, with largest temperature anomalies over a zonal band across the southern Tasman Sea and Chatham Rise, and continuing farther east, following roughly the path of the Subtropical Front (Behrens & Bostock 2022). Most of this warming has been attributed to blocking high pressure conditions over NZ (Fig. 9), which reduced the wind-driven vertical ocean mixing and enhanced incoming solar radiation, causing the near-surface waters to warm rapidly. Furthermore, the reduced westerly winds, associated with the blocking high pressures, caused anomalous southward Ekman transports, and likely contributed to the zonal band of the highest positive temperature anomalies. Note that a small southward displacement in the location of the Subtropical Front, due to weaker westerly winds, would coincide with a positive anomaly (Behrens & Bostock 2022). The spatial pattern of top 50m temperature anomalies for the summers of 2021/22 and 2022/23 are associated with north easterly wind anomalies and characterized by generally weaker

westerly winds, with temperatures anomalies well above 2°C along the west coast of the South Island associated with reduced coastal upwelling (Chiswell and O'Callaghan (2021). In 2021/22 the largest temperature anomalies spread from the south of Tasmania to the northeast of NZ, rather than following the zonal band of the previous years. The reduced coastal upwelling resulted in sponges bleaching (Bell et al. 2024). In summer 2022/23 negative anomalies emerge in the northern Tasman Sea and the largest warming again spreads zonally across the southern Tasman Sea south to the east of the Chatham Rise.

While the summer of 2022/23 top 50m area-average anomalies did not exceed previous records of 2017/18, the top 300m ocean heat content did exceed previous summer records (Fig. 10f) as part of an ongoing increase. This reflects that NZ's waters were also substantially warm below the mixed layer (Fig. 5 and 6) and some of the warming might not coincide with positive anomalies at the surface.

3.5 Recurrence interval of heatwaves

Based on the temperature distribution up to 1934/35 (Fig. 10a), the 1934/35 summer was very rare, with a probability of occurrence of 0.003, or an ERI of around 320 years. Using the 1957-2023 distribution, the 1934/35 event is still relatively uncommon, with an estimated ERI of around 30 years. For the recent extreme warm summers, compared to the temperature distribution from 1957 to 2023 (Fig. 10b), the three most recent have ERIs in the range of 25-40 years while 2017/18 has an ERI of around 100 years.

4.0 Consequences and impacts

Such large departures from normal in the circulation and temperatures had consequences, and here we briefly consider impacts on glaciers and snow cover, grapes, and sponges in the ocean.

314 *4.1 Glacier ice volume and Seasonal Snow*

315 Ice volume loss in the Southern Alps for the small and medium glaciers was estimated to be
316 0.7 km^3 volume in 1934/35, 2.6 km^3 in 2017/18, and 2.5 km^3 in 2018/19 (Fig 11). The total loss from
317 2017/18 to 2020/21 was 7.6 km^2 2017 to 2021; 20% of the total ice volume of the Southern Alps
318 compared with March 2017 (Chinn 2001). The 2017 – 2021 period represents the largest ice loss in
319 any 5-year period since 1949 (Salinger et al. 2021). Total ice volume declined from 42 km^3 to 34
320 km^3.

321 Generally, all the five AHW years had the fastest observed snowmelt. The 1934-1935 snow
322 year was remarkable. Water stored as seasonal snow reached a maximum that was just below average
323 at 402mm water equivalents (w.e.) in mid-October, based on SnowSim model estimates. Rapid
324 snowmelt began in mid-November. All snow had disappeared by 11 January, the third earliest date
325 for the 1930-2023 period (Fitzharris and Garr, 1995; de Latour, 1999) with a melt rate over this
326 period of 6.5mm/d w.e., the highest of the five summers. For the other four recent heatwave summers
327 (Fig. 12) the melt rate was very rapid once commenced from November and accelerated to more than
328 5.0 mm/d w.e. All seasonal snow had disappeared in the 2017-18 snow year by early January, albeit
329 from a below average maximum. The snow year 2018-19 had a near average maximum snow but it
330 had all melted by mid-February. More remarkable was the 2022-2023 snow year. Maximum
331 accumulation was well above average and occurred early (Mid-September); thereafter melt
332 accelerated so that all seasonal snow was gone by early February.

333 *4.2 Agriculture Grapes*

334 Progressive advances in phenology reflect differences in seasonal temperatures since 1943
335 (Salinger et al. 2020). The temperature during flowering influences pollen tube growth rate (Staudt
336 1982) and largely determines fruit set and in turn berry number per bunch in the current season and
337 inflorescence initiation in the subsequent season (Trought 2005; Zhu et al. 2020). Seasonal
338 differences in Marlborough (42^{o}S, 174^{o}E the primary wine production area in NZ) Sauvignon blanc

grapevine yield ranged from a high of 15.2 Tonnes/hectare (T/ha) in 2022 to a low of 10.3 T/ha in 2021. The differences largely reflected seasonal changes in bunch mass, which in turn reflected the berry number per bunch.

The mean local temperatures for over flowering in 2014 and 2022 (the years with the highest yields, 15.8 and 15.2 T/Ha respectively) were 18.1 and 18.9°C respectively, while those for the years with the lowest yield (10.8 and 10.3 T/Ha respectively in 2015 and 2021) were 17.9 and 16.8°C respectively. The seasonal differences were amplified by cold periods in the middle of flowering in both the 2015 and 2021 vintages (Figure 13) and mean daily temperatures did not exceed 15°C. Rainfall variability does not have any discernible impact.

4.3 Marine ecosystems

There were impacts of the MHW on some organisms, but records are scarce. In northeastern NZ during 2022, sponge necrosis was recorded at depths between 1–20m. Up to 45% of sponges observed in this region showed signs of necrosis. In the Fiordland region, widespread sponge 'bleaching' of *Cymbastella lamellata* was first reported during the 2021/22 marine heatwaves (Bell et al. 2022). Further sponge bleaching was reported in 2023 (Bell, 2024) and diver based underwater visual census in Doubtful Sound with 10 and 20 m depth found evidence of bleaching in >90% of sponges encountered, with sponge densities greater than 10 sponges per m^2, and bleaching down to 50 m.

The four very intense coastal MHW since 2017 caused major species disruptions in coastal marine ecosystems where mortalities led to local extinctions and shifts in biodiversity (Bell et al. 2024) and death of kelps and sponges in the fiords. Further afield the MHW caused movement of pelagic fisheries to out of range occurrence (Salinger et al 2018, 2020), and mortality of marine aquaculture (Salinger et al. 2023). There is no doubt other impacts have occurred that have not been observed and documented here.

5. Discussion: Mechanisms and Extremes

Salinger et al. (2020) note the NZ regional temperature signal, NZEEZT, showed an increase of 0.8°C representing the magnitude of the warming signal for the 1900-2015 period. Climate teleconnections were identified on a seasonal to decadal basis by Salinger et al. (2020). After AGW the most significant climate teleconnection is the SAM on a centennial scale. On interannual to interdecadal timescales the ENSO and the IPO are the most important. After detrending for AGW, the SAM correlation values are lower whereas the IPO and SOI correlation values strengthen, demonstrating the importance of these on interannual to decadal timescales, especially the La Niña phase of ENSO.

Thus, on a monthly to seasonal basis, positive (+1.0 to 2.2) SAM phases produce above average temperatures (+0.7° to 1.1ºC) (Table 1) (Kidston et al. 2009). A positive Southern Oscillation Index (SOI), signifying La Niña, produces above average seasonal temperature whereas a negative SOI, El Niño conditions, generally cause below average seasonal NZ temperatures (Gordon, 1986). During positive (negative) IPO phases, SST anomalies are negative (positive) in the NZ sector, and similarly with land surface air temperatures (Power et al., 1999).

With temperatures warming from 1900 – 2020, SAM becoming progressively positive and it is only a matter of time before AHW/MHW conditions are compounded, resulting in other extremes (e.g. days ≥25 or ≤0ºC, TX90p, TN10p). The change in the IPO and the negative phase produces more frequent La Niña phases of ENSO tipping the region into more MHW/AHW heatwave events.

The extreme statistic HWF has shown high values for the heatwaves - together, the impacts are magnified when the combination of extreme events cascade to rapid loss of permanent snow and ice on the Southern Alps, fast melting of seasonal snow, advance of the viticulture season, and marine ecosystem mortality.

Heatwaves are becoming a major impact of global warming, as noted by the Intergovernmental Panel on Climate Change 6th Assessment Report (Masson-Delmotte et al. 2021), indicating likely increases in unusually warm days and nights across most continents, and several occurrences of MHWs in 2019 (Blunden and Boyer 2020). The unprecedented heatwave in the 2017/18 austral summer, coupled with a combined AHW/MHW event (Salinger et al 2019a) was one example.

The results have highlighted the extremes in the extended austral summer seasons of 1934/35, 2017/18, 2018/19, 2021/22 and 2022/23. The area-averages reveal that the latter four events identified have been the warmest around NZ over the 32-year record (Fig. 9e) with peak temperature anomalies tending to occur towards the end of summer and autumn (February-April). In the estimated future distributions (Min. Environment 2018) with 1.5° or 2°C warming (added to the 1870-1920 distribution), such summers would be common even under 1.5°C warming, with ERIs of 2-3 years. Under 2°C warming, those years would all be occurring as cool years, approximately twice per decade. Under the current climate warming trajectory this would be reached around the 2040s to 2050s (Mullan et al. 2016). Hence, this behaviour follows climate change projections where positive anomalies disproportionally extend into autumn as the ocean warms under climate change (Behrens et al. 2022). Although Perkins-Kirkpatrick et al. (2018) suggests that the 2017/18 MHW would have been "virtually impossible" without an anthropogenic influence, the 1934/35 event indicates that a similar episode occurred in the past where regional temperatures were 0.7ºC cooler than the 1991-2020 climatology.

The estimated recurrence interval reduces from 1 in 300-year AHW event during the 1930s climate to a 1 in 25-year event for the most recent decade, which coincides with AGW of ~0.8 ºC from 1900 - 2015. These are consistent with the results of Vargo et al (2020), who applied event attribution methods to document direct links between anthropogenic and ice-mass loss in the Southern Alps, targeting the highest mass-loss years (2011 and 2018). The study estimates extreme

mass loss was at least six times (2011) and ten times (2018) (>90% confidence) more likely to occur with anthropogenic forcing than without. This increased likelihood is driven by present-day temperatures ~1.0 °C above the pre-industrial average, confirming a connection between anthropogenic emissions and high annual ice loss.

6. Conclusions

The 2017–18 and 2018–19 summers exhibited very large SST anomalies in the Tasman Sea, with AHW and MHW heat wave conditions reaching 4–5 °C above normal in 2017–18 and 2.5 °C above normal in 2018–19. These anomalous warm spells were the result of prolonged periods of calm winds associated with blocking atmospheric high-pressure systems to the east of NZ (Behrens et al. 2020; Salinger et al. 2018, 2023). These warm events are typically associated with summers and are constrained to the upper 40 m or so of the water column — corresponding to the depth of the summer mixed layer.

Cool events occur year-round in the Tasman Sea/NZ area and can extend down to more than 100 m — corresponding to the depth of the winter mixed layer. An approximately 30 m deep layer of warm water formed in November 2017 and persisted. The similar but weaker warm event in summer 2018–19 peaked at an anomaly of ~+2.5 °C. It was also mixed down into the water column by winds once the atmospheric blocking high broke down.

Five such austral summer MHW and AHW events have now occurred – in decreasing order of magnitude 2017/18, 1934/35, 2022/23, 2018/19 and 2021/22. The heatwaves had very similar atmospheric and oceanic footprints, covering all the land area, the entire central and south Tasman Sea and across to 180ºE in the southwest Pacific. Mid-tropospheric (500-hPa) anomalies were very similar with strong blocking in the Tasman Sea and extending southeast of NZ. The 2017/18 and 2018/19 events appeared to be predominantly atmospherically driven with blocking high pressure conditions over NZ associated with SAM, reducing the wind-induced vertical ocean mixing and

enhanced incoming solar radiation and rapid near-surface waters warming. Ocean analysis shows that the warming in upper part of the oceans were spread in a zonal band around NZ associated with blocking high pressure conditions reducing the wind-induced vertical ocean mixing and enhancing solar incoming radiation.

For 2021/22 and 2022/23, a pattern associated with La Niña conditions, featured the largest temperature anomalies from south of Tasmania to the northeast of NZ. Behrens et al. (2019) note each MHW is unique, either atmospherically driven, or a combination of atmospheric surface warming and oceanic heat advection. Trenberth et al. (2019) suggest that MHWs in the south Tasman Sea region may be linked to heat transports from the tropical South Pacific to the East Australia Current instead of through the Indonesian throughflow. Increased advection of warmer waters into the Tasman Sea is likely to be at the expense of a weak heat transport between the Pacific and Indian basins, as the inter-basin flow relaxes with weaker easterly trade winds during El Niño years.

The relationship of MHWs with positive SAM phase is consistent with Gregory et al (2024), whereas La-Niña conditions are the prime climate driver for the South Island of NZ and to the east for combined AHWs and MHWs. There is a trend towards the positive SAM resulting in higher MSLPs in the NZ region, but this depends on interplay with stratospheric ozone recovery (Arblaster et al. 2011). Upon this background, notable climate extremes have occurred including AHW and MHW (Salinger at. 2018, 2020 and 2023), extremes of temperature and rainfall (Salinger and Griffiths 2001) and drought (Salinger and Porteous 2014), and other extremes (Dean et al. 2013, Harrington et al. 2016, Harrington et al. 2014, Reid et al. 2021).

Projected circulation changes for the late 21st century (Mullan et al. 2016) show MSLP increases during DJF, especially to the southeast of NZ. The airflow over the country becomes more northeasterly, and at the same time associated with more (possibly blocking) anticyclones and lacking in troughs. Given that the Tasman Sea mixed layer heat content anomalies in recent years

have been above average, it appears likely that human-induced warming has played a significant role in the two recent coupled MHW/AHW.

There has been a marked increase in frequency of the NZ regional AHWs after 2016 from a return interval of a 300-year event in the pre-1935 climate, to an ERI of about 25 years for the 1956-2023 climate. This suggests that with AGW of at least 0.7ºC accompanied by a positive trend in SAM during the 20th century and a change in the mode of the IPO to the negative phase, conditions were ripe for the development of heat wave conditions. Once the prolonged La Niña phase of ENSO occurred these increased the odds of the present wave of compound AHW/MHW extremes to occur, and further extreme events. The higher frequency of such events produced large impacts on the NZ cryosphere, and terrestrial and marine ecosystems have been highly disrupted.

It is not a surprise that the compound AHW/MHWs have had substantial consequences. Massive ice loss occurred in the Southern Alps. Ice loss in small and medium glaciers has been estimated to range from about 2 to 4.5 km^3 w.e. in each event. Across the three recent AHW/MHW seasons from 2017 to 2021, there was an accumulated ice volume loss of 20% of the 2017 volume. The massive ice losses have been linked to AGW. Seasonal snow melt rates have been remarkable. For winegrapes, an advance in phenology caused by a progressive 0.5°C increase in temperatures and heat waves have advanced Marlborough Sauvignon blanc harvest dates and short-term changes in seasonal temperature over flowering resulted in 50% differences in yield. Further, the four very intense coastal MHWs since 2017 caused major species disruptions in coastal marine ecosystems and pelagic fisheries.

Author Contributions

M James Salinger: Conceptualization; data curation; formal analysis; visualization; writing review and editing, project administration; investigation; methodology; resources. Kevin E. Trenberth: Visualization; conceptualization, writing – review and editing, supervision, validation. Howard J Diamond: Data curation, formal analysis, methodology, visualization, writing – original draft and edits. Erik Behrens: Data curation, methodology, software, validation, analysis and writing – original draft. B Blair Fitzharris: Data curation, visualization, writing – original draft. Nicholas Herold: Data curation, software, writing – review and editing. Robert O Smith: Data curation, formal analysis, visualization, writing – review and editing. Phil J Sutton: Data curation, formal analysis, visualization. Michael C T Trought: Formal analysis, writing – review and editing.

Data and Acknowledgments

Monthly SST observations were obtained from Ocean sub-surface temperature Argo profiles (Jayne et al, 2017) were extracted for the eastern Tasman Sea (160-172°E, 35-45°S) accessed August 2023. Climate data were accessed from the NIWA Climate Database (www.cliflo.niwa.co.nz) for daily temperature, rainfall and mean sea level pressure (accessed August 2023). For precipitation 5-day annual maximum precipitation was examined using the Virtual Climate Station Network (VCSN) of NIWA (https://niwa.co.nz/climate/our-services/virtual-climate-stations).

For large-scale circulation and monthly to decadal modes of variability the following were used: the Fogt et al. (2009) SAM (https://polarmet.osu.edu/ACD/sam/sam_recon.html -Accessed August 2023 combined with the Marshall (2003) SAM index (https://legacy.bas.ac.uk/met/gjma/sam.html - Accessed January 2024, the Southern Oscillation Index (SOI) (Standardized Tahiti -- Standardized Darwin) based on monthly standardization (Trenberth 1984) was provided by Climate Analysis Section, NCAR, Boulder, USA (Accessed 18-January-2024.https://climatedataguide.ucar.edu/sites/default/files/2022-10/SOI.darwin.txt), and for the IPO Tripole Index (Henley et al. 2015 – Accessed November 2023).

To also quantify oceanic changes around NZ we use the ORAS5 reanalysis (Zuo et al. 2019) product, which is freely available, regularly updated and distributed through https://cds.climate.copernicus.eu/cdsapp#!/dataset/reanalysis-oras5?tab=form. This global model data assimilation provides physical ocean properties as monthly means from 1958 to present on a global 0.25° horizontal grid with 75 vertical z-levels. The Argo data were collected and made freely available by the International Argo Program and the national programs that contribute to it (http://www.argo.ucsd.edu,

http://argo.jcommops.org)and is part of the Global Ocean Observing System. The oceanic analyses in this paper were supported through funding from the Ministry of Business, Innovation and Employment (MBIE, 2023) via the Deep South National Science Challenge (C01X1902). The sub-surface temperature and SST data were collected as part of the MBIE funded Coastal Acidification: Rate, Impacts and Management (CARIM) project, provided by Kim Currie. MST was funded by the Brian Mason Trust (Impact of an unprecedented marine heatwave). PMS was funded by MBIE contract CAWX1801. Bay of Plenty kororā research was obtained under wildlife authorities (48462-FAU & 81642-DOA), thanks to the Department of Conservation, local iwi (Ngai Te Rangi, Ngati Ranginui and Ngati Pukenga) and Tauranga City Council for granting permissions and land use access.

Tasman Glacier end of summer snow line data as well as the proglacial lake and down wasting of volume for the 12 large glaciers were provided by the late Dr Trevor Chinn. Subsequent End of Summer Snowline surveys from 1977 until 2021 (Min. of Business and Innovation & Employment 2023) provided mass balance data from the 50 index glaciers.

Marlborough temperature data were sourced from the regional meteorological station (41.48°S, 173.95°E) and the NIWA climate database(www.cliflo.niwa.co.nz). Dr James Renwick fitted the generalized extreme value distribution for the periods 1871-1935 and 1957-2022 and calculated the expected probability of occurrence and the estimated return interval (ERI) of the extreme temperatures.

Data availability statement

All datasets used in this study are available from their respective public domain sources

Conflict of Interest Statement

The authors declare no conflicts of interest.

References

Arblaster, J.M., Meehl, G.A. & Karoly, D.J. (2011) Future climate change in the Southern Hemisphere: Competing effects of ozone and greenhouse gases. *Geophysical Research Letters*, 38(2), https://doi.org/10.1029/2010GL045384

Alexander, L., & Herold N. (2015) *ClimPACTv2 Indices and Software*. A document prepared on behalf of the Commission for Climatology (CCl) Expert Team on Sector-Specific Climate Indices (ET-SCI). https://github.com/ARCCSS-extremes/climpact2/blob/master/ClimPACTv2_manual.pdf.

Behrens, E. & Bostock, H.(2022) The response of the Subtropical Front to changes in the Southern Hemisphere Westerly Winds–Evidence from models and observations. *Journal of Geophysical Research: Oceans*, e2022JC019139 https://doi.org/10.1029/2022jc019139

Behrens, E., Williams, J., Morgenstern,O., Sutton, P., Rickard, G., & Williams,M. J. M. (2020) Local grid refinement in New Zealand's earth system model:Tasman Sea ocean circulation improvements and super-gyre circulation implications. *Journal of Advances in Modeling Earth Systems,*12, https://doi.org/10.1029/2019MS001996

Behrens, E., Rickard, G., Rosier, S., Williams, J., Morgenstern, O., & Stone, D. (2022) Projections of future marine heatwaves for the Oceans Around New Zealand Using New Zealand's Earth System Model. *Frontiers in Climate*, 4, 798287 https://doi.org/10.3389/fclim.2022.798287

Behrens, E., Fernandez, D., & Sutton, P (2019) Meridional Oceanic Heat Transport Influences Marine Heatwaves in the Tasman Sea on Interannual to Decadal Timescales. *Frontiers Marine Science,* 6, 228 https://doi.org/10.3389/fmars.2019.00228

Bell, B., H. Hersbach, H., Simmons, A., Berrisford, P., Dahlgren, P., Horányi, A., Muñoz-Sabater, J., Nicolas, J., Radu, R., Schepers, D., Soci, C., Villaume, S., Bidlot, J-R., Haimberger, L., Woollen, J., Buontempo, C & Thépaut , J-N. (2021) The ERA5 global reanalysis: Preliminary extension to 1950. *Q J R Meteorol Soc*, 147(741), 4186-4227 https://doi.org/10.1002/qj.4174

554 Bell, J.J., Smith, R.O., Micaroni, V., Strano F., Balemi, C.A., Caiger, P.E., Miller, K.I., Spyksma,
555 A.J.P., & Shears, N.T. (2022) Marine heat waves drives bleaching and necrosis of temperate
556 sponges. *Current Biology,* https://doi.org/10.1016/j.cub.2022.11.013
557 Bell, J.J., Micaroni, V., Strano, F., Ryan, K.G., Mitchell, K., Mitchell, P., Wilkinson, S., Thomas, T.,
558 Batchiar, R., Smith, R.O. (2024) Marine heatwave-driven mass mortality and microbial
559 community reorganisation in an ecologically important temperate sponge. *Global Change*
560 *Biology*, 30(8), https://doi.org/10.1111/gcb.17417
561 Bowen, M. M., Sutton, P. J., & Roemmich, D. (2006) Wind-driven and steric fluctuations of sea
562 surface height in the southwest Pacific. *Geophysical Research Letters,* 33(14), L14617
563 https://doi.org/10.1029/2006gl026160
564 Blunden, J. & T. Boyer, Eds. (2020) State of the Climate in 2020. *Bulletin of the American*
565 *Meteorological Society*, 102 (8) Si–S475,
566 https://doi:10.1175/2021BAMSStateoftheClimate.1.
567 Clare, G. R., Fitzharris, B.B, Chinn, T.J.H & Salinger, M.J. (2002) Interannual variation in end-of-
568 summer snowlines of the Southern Alps of New Zealand, and relationships with Southern
569 Hemisphere atmospheric circulation and sea surface temperature patterns. *Int. J. Climatol.* 22,
570 107–120 https:// doi.org: 10.1002/joc.722
571 Cheng, L. J., and Coauthors, 2024: New record ocean temperatures and related climate indicators in
572 2023. *Adv. Atmos. Sci.*, https://doi.org/10.1007/s00376-024-3378-5.
573 Chinn, T.C., Fitzharris, B.B., Willsman, A and **Salinger. J**. Annual Ice Volume Changes 1976-2008
574 for the New Zealand Southern Alps. *Global and Planetary Change,* 92.
575 Doi:10.1016/j.gloplacha.2012.03.002
576 Chiswell, S.M. & O'Callaghan, J. M. (2021): Long-term trends in the frequency and magnitude of
577 upwelling along the West Coast of the South Island, New Zealand, and the impact on primary

production, New Zealand Journal of Marine and Freshwater Research, https://doi.org/10.1080/00288330.2020.1865416

Chiswell, S.M., Bostock, H.C., Sutton, P.J.H., & Williams, M.J.M. (2015) Physical oceanography of the deep seas around New Zealand: a review, *New Zealand Journal of Marine and Freshwater Research*, https://doi.org/10.1080/00288330.2014.992918.

Dean, S. M., Rosier, S., Carey-Smith, T., & Stott, P. A. (2013) The role of climate change in the two-day extreme rainfall in Golden Bay, New Zealand, December 2011 [in "Explaining Extreme Events of 2012 from a Climate Perspective"]. *Bulletin of the American Meteorological Society*, 94(9), S61-S63 https://www.jstor.org/stable/26218715

de Lautour, S. 1999. The climatology of seasonal snow. MSc Thesis, Department of Geography, University of Otago.

Dowson, A.J., Sirguey, P. & Cullen, N.J. (2020). Variability in glacier albedo and links to annual mass balance for the gardens of Eden and Allah, Southern Alps, New Zealand. *The Cryosphere,* 14(10) 3425-3448. https://doi.org/10.5194/tc-14-3425-2020

Fitzharris, B., & Garr, G.E. (1995) Simulation of past variability in seasonal snow in the Southern Alps, *New Zealand. Annals of Glaciology*, 21, 377-382. https://doi.org/10.3189/S0260305500016098.

Fogt, R.L., Perlwitz, J., Monaghan, A.J., Bromwich, D.H., Jones, J.M., & Marshall, G.J. (2009) Historical SAM variability. Part II: Twentieth-century variability and trends from reconstructions, observations, and the IPCC AR4 models. *Journal of Climate*, 22, 53465365 https://doi.org/10.1175/2009JCLI2786.1.

Gordon, N.D. (1986) The Southern Oscillation and New Zealand weather, *Monthly Weather Review,* 114, 371 – 387 https://doi.org/10.1175/1520- 0493(1986)1142.0.CO;

602 Graham R.M., De Boer, A.M. (2013) The Dynamical Subtropical Front. *J. Geophys. Res.,* 118, 5676–
603 5685. https://doi.org/10.1002/jgrc.20408
604 Gregory, C.H., Holbrook, N.J., Marshall, A.G. & Spillman, C.M. (2023) Atmospheric drivers of
605 Tasman Sea marine heatwaves. *Journal of Climate*, 36**,** 5197-5214.
606 https://doi.org/10.1175/JCLI-D-22-0538.1.
607 Gregory, C.H., Holbrook, N.J., Marshall, A.G. et al. (2024) Sub-seasonal to seasonal drivers of
608 regional marine heatwaves around Australia. *Clim Dyn* https://doi.org/10.1007/s00382-024-
609 07226-x
610 Harrington, L. J., Gibson, P. B., Dean, S. M., Mitchell, D., Rosier, S. M., & Frame, D. J. (2016)
611 Investigating event-specific drought attribution using self-organizing maps. *Journal of*
612 *Geophysical Research: Atmospheres*, 121(21), 12,766-712,780
613 https://doi.org/10.1002/2016JD025602
614 Harrington, L. J., Rosier, S., Dean, S. M., Stuart, S., & Scahill, A. (2014) The role of anthropogenic
615 climate change in the 2013 drought over North Island, New Zealand [in "Explaining
616 Extremes of 2013 from a Climate Perspective"] *Bulletin of American Meteorological Society*,
617 95(9), S45-S48. https://doi.org/10.1002/2016JD025602
618 Henley, B.J., Gergis, J., Karoly, D.J., Power, S.B., Kennedy, J., & Folland, C.K. 2015. A Tripole
619 Index for the Interdecadal Pacific Oscillation. *Climate Dynamics*, 45 (11-12), 3077-3090
620 http://dx.doi.org/10.1007/ s00382-015-2525-1. Accessed on 05 27 2019 at
621 https://www.esrl.noaa.gov/psd/data/timeseries/ IPOTPI
622 Hobday, A., Alexander, L.V., Perkins, S.E., Smale, D.A., Straub, S.C., Oliver, E.C.J., Benthuysen,
623 J.A., Burrows, M.T., Donat, M.G., Feng, M., Holbrook, N.J., Moore, P.J., Scannell, H.A., Sen
624 Gupta, A., & Wernberg, T. (2016) A hierarchical approach to defining marine heatwaves.
625 *Progress in Oceanography* 141, 227–238 https://doi.org/10.1016/j.pocean.2015.1012.1014.
626 Outcome of Workshop #1

627 Hobday, A.J., Oliver, E.C.J., Sen Gupta, A., Benthuysen, J.A., Burrows, M.T., Donat, M. G.,
628 Holbrook, N.J., Moore, P.J., Thomsen, M.S., Wernberg, T & Smale., D.A. (2018)
629 Categorizing and naming marine heatwaves. *Oceanography,* 31(2), 162–173
630 https://doi.org/10.5670/oceanog.2018.205
631 Holbrook, N.J., Sen Gupta A., Oliver, E.C.J., Hobday, A.J., Benthuysen, J.A., Scannell, H.A.,
632 Smale, D.A., Wernberg, T. (2020) Keeping pace with marine heatwaves. *Nat Rev Earth*
633 *Environ* 1, 482–493 https://doi.org/ 10.1038/s43017-020-0068-4
634 Huang, B., Liu, C., Banzon, V., Freeman, E., Graham, G., Hankins, B., Smith, T., & H.-M. 2020.
635 Improvements of the Daily Optimum Interpolation Sea Surface Temperature (DOISST)
636 Version 2.1, *Journal of Climate,* 34, 2923-2939 https://doi.org/10.1175/JCLI-D-20-0166.1
637 Huang, B., Thorne, P.W., Banzon, V.F., Boyer, T., Chepurin, G., Lawrimore, J.H., Menne, M.J.,
638 Smith, T.M., Vose, R. S & Zhang, H-M. (2017) Extended Reconstructed Sea Surface
639 Temperature version 5 (ERSSTv5), Upgrades, validations, and intercomparisons. *J. Climate*,
640 30(20), 8179–8205 https://doi.org/ 10.1175/JCLI-D-16-0836.1
641 Hunke, E., Lipscomb, W., Jones, P., Turner, A., Jeffery, N. & Elliott, S. (2017) CICE, The Los
642 Alamos Sea Ice Model (https: //doi.org/10.2172/1346837)
643 IPCC, (2021) *Climate Change 2021: The Physical Science Basis. Contribution of Working Group I*
644 *to the Sixth Assessment Report of the Intergovernmental Panel on Climate Change*[Masson-
645 Delmotte, V., P. Zhai, A. Pirani, S.L. Connors, C. Péan, S. Berger, N. Caud, Y. Chen, L.
646 Goldfarb, M.I. Gomis, M. Huang, K. Leitzell, E. Lonnoy, J.B.R. Matthews, T.K. Maycock, T.
647 Waterfield, O. Yelekçi, R. Yu, and B. Zhou (eds.)]. Cambridge University Press, Cambridge,
648 United Kingdom and New York, NY, USA https://doi:10.1017/9781009157896.
649 Jayne, S.R., Roemmich, D., Zilberman, N., Riser, S.C., Johnson, K.S., Johnson, K.C., & Piotrowicz,
650 S.R. (2017) The Argo Program: present and future, *Oceanography,* 30, 18–28
651 https://doi.org/10.5670/oceanog.2017.213

652 Keable, M., Simmonds, I., & Keay, K. (2002) Distribution and temporal variability of 500 hPa
653 cyclone characteristics in the Southern Hemisphere. *International Journal of Climatology.* 22
654 (2), 131-150 https://doi.org/10.1002/joc.728
655 Kidson, E. (1935). The summer of 1934/35 in New Zealand. *New Zealand Meteorological Office*
656 *Note*, 16 1- 12.
657 Kidson, J.W. (2000) An analysis of New Zealand synoptic types and their use in defining weather
658 regimes. *Int. J. Climatol.,* 20 (3) 299-316, https://doi.org/10.1002/(SICI)1097-
659 0088(20000315)20:3<299::AID-JOC474>3.0.CO;2-B
660 Kidson, J. W., & Renwick, J.A. (2002) Patterns of convection in the tropical Pacific and their
661 influence on New Zealand weather. *Int. J. Climatol.,* 22, 151–174 https://doi.org:
662 10.1002/joc.737
663 Kidston, J., Renwick, J.A., and McGregor, J., 2009. Hemispheric-scale seasonality of the Southern
664 Annular Mode and impacts on the climate of New Zealand. *Journal of Climate,* 22, 4759-
665 4770 https://doi.org/ 10.1175/JCLI-D-11-00474.1
666 Lorrey, A.M., Vargo, L., Purdie, H., Anderson, B., Cullen, N.J., Sirguey, P., Mackintosh, A.,
667 Willsman, A., Macara, G & Chinn, W. Southern Alps equilibrium line altitudes: four
668 decades of observations show coherent glacier–climate responses and a rising snowline trend.
669 *J. Glaciology* 68 (272), 1127-1140. https://doi.org/10.1017/jog.2022.27
670 Madec, G. and the NEMO System Team, 2023. *NEMO Ocean Engine Reference Manual, Zenodo,*
671 https://doi.org/10.5281/zenodo.8167700
672 Marshall, G. J., 2003: Trends in the southern annular mode from observations and reanalyses.
673 *Journal Climate*, **16**, 4134–4143. https://doi.org/10.1175/1520-
674 0442(2003)016<4134:TITSAM>2.0.CO;2
675 Marlow, J., Davy, S.K., Shaffer, M. et al. (2018) Bleaching and recovery of a phototrophic
676 bioeroding sponge. *Coral Reefs* 37, 565–570 https://doi.org/10.1007/s00338-018-1680-3

677 Marshall, G.J. (2003) Trends in the southern annular mode from observations and reanalyses.
678 *Journal of Climate*, 16: 4134–4143.
679 https://doi.org/10.1175/15200442(2003)016<4134:TITSAM>2.0.CO;2.
680 Menary,M.B. et al. (2018) Pre-industrial control simulations with HadGEM3-GC3.1 for CMIP6.
681 *J. Adv. Model. Earth Syst.* 10 2049–3075 https://doi.org/10.1029/2019MS001995
682 Ministry of Business, Innovation and Employment (2023). *New Zealand Glacier Monitoring: End of*
683 *summer snowline survey 2021.* 157 pp.
684 Mullan, A B; Stuart, S., J Hadfield, M.G & Smith, M. J. (2010) Report on the Review of NIWA's
685 'Seven-Station' Temperature Series. NIWA Information Series No. 78. 175 p.
686 https://niwa.co.nz/sites/niwa.co.nz/files/import/attachments/Report-on-the-Review-of-
687 NIWAas-Seven-Station-Temperature-Series_v3.pdf
688 Pan, Y., L. Cheng, K. von Schuckmann, K. E. Trenberth, G. Li, J. Abraham, Y. Liu, V. Gouretski, Y.
689 Yu, H. Liu, and C. Liu, 2023: Annual cycle in upper ocean heat content and the global energy
690 budget. *J. Climate*, 36, 5003-5026. https://doi.org/10.1175/JCLI-D-22-0776.1
691 Perkins, S.E. & Alexander, L.V. 2013. On the measurement of heat waves. *J. Climate* 26(13) 4500 –
692 4517. https://doi.org/ 10.1175/JCLI-D-12-00383.1
693 Perkins-Kirkpatrick S.E., King, S.E., Cougnon. A.D., Grosese, E.A., Oliver, M.R., Holbrook, N.J.,
694 Lewis, S.C. &, Pourasghar, F. (2018) The role of natural variability and anthropogenic
695 climate change in the 2017/18 Tasman Sea marine heatwave. Bulletin of American
696 Meteorological Society http://doi.org/10.1175/BAMS-D-18-0116.1
697 Power, S., Casey, T., Folland, C. et al. (1999) Inter-decadal modulation of the impact of ENSO on
698 Australia. *Climate Dynamics* 15, 319–324 (1999) https://doi.org/10.1007/s003820050284
699 Reid, K. J., Rosier, S. M., Harrington, L. J., King, A. D., & Lane, T. P. (2021) Extreme rainfall in
700 New Zealand and its association with Atmospheric Rivers. *Environmental Research Letters*,
701 16(4), 044012 https://doi.org/10.1088/1748-9326/abeae0

Ridgway, K.R, Dunn, J. R. & Wilkin, J. L. (2002) Ocean interpolation by four-dimensional least squares -Application to the waters around Australia *J. Atmos. Ocean. Technol.* 19 1357–75 https://doi.org/10.1175/1520-0426(2002)019<1357:OIBFDW>2.0.CO;2

Roemmich, D; Gilson, J K; Davis, R; Sutton, P; Wijffels, S; Riser, S (2007) Decadal Spin-up of the South Pacific Subtropical Gyre. *Journal of Physical Oceanography* 37, 162–173 https://doi.org/10.1175/JPO3004.1

Roemmich, D; Gilson, J; Sutton, P & Zilberman, N (2016) Multidecadal Change of the South Pacific Gyre Circulation. *Journal of Physical Oceanography* 46, 1871–1883 https://doi.org/10.1175/JPOD-15_0237.1

Roemmich, D; Sutton, P Saha, S. et al (2006) The NCEP climate forecast system. *Journal of Climate* 19, 3483–3517 https://doi.org/10.1175/JCLI-D-12-00823.*1*

Salinger, J., Behrens, E., Mullan, A. B., Diamond, H. J., Renwick, J.A., Sirguey, P.,, Smith, R. O; Trought, M., C. T; Alexander, L. V., Cullen, N. J., Fitzharris, B. B., Hepburn, C. D., Parker, A. K & Sutton, P. J (2018) The unprecedented coupled ocean-atmosphere summer heatwave in the New Zealand Region 2017/18: Drivers, Mechanisms and Impacts. Environmental Research Letters 14, 044023 https://doi.org/10.1088/1748-9326/ab012a.

Salinger, M.J., Diamond, H.J. & Renwick, J.A. (2020) Surface temperature trends in New Zealand and surrounding oceans 1870 – 2019 (2020) *Weather and Climate* 40**,** 32-50 https://www.jstor.org/stable/10.2307/27031378

Salinger, M.J. & Griffiths, G. (2001) Trends in annual New Zealand daily temperature and rainfall extremes. *International Journal of Climatology*, 21, 1437-1452 https://doi.org/10.1002/joc.694

Salinger, M.J. & Porteous, A.S. (2014) New Zealand Climate: Patterns of drought 1941/42 – 2012/13. *Weather and Climate* 34, 2-19 https://doi.org/10.2307/26169741

Salinger, M.J., Renwick, J. A & Mullan A.B. (2001) Interdecadal Pacific Oscillation and South Pacific climate. *Int. J. Climatol.,* 21, 1705–1721 https://doi.org/10.1002/joc.691

Salinger, M J; Renwick, J., Diamond, H. J., Behrens, E., Fernandez, D., Mullan, A. B., Smith, R. O., Parker, A. K., Johnstone, P., Teixeira, E., Woodward, A., Sirguey, P., Cullen, N. J., Fitzharris, B. B., Herold, N., Hales, S., Hepburn, C. D., Trought, M. C. T & Sutton P. J. (2020) Unparalleled coupled ocean-atmosphere summer heatwaves in the New Zealand region: drivers, mechanisms and impacts. *Climatic Change* 162, 485–506 https://doi.org/10.1007/s10584-020-02730-5

Salinger, M.J., Diamond, H.J., Bell, J., Behrens, E., Fitzharris, B.B., Herold, N., McLuskie, M., Parker, A.K., Ratz, H., Renwick, J.A., Scofield, C., Shears, N.T., Smith, R.O., Sutton, P.J. & Trought, M.C.T. Coupled ocean-atmosphere summer heatwaves in the New Zealand region: An update. (2023). *Weather and Climate* 42, 18-41 https://doi.org/10.2307/27226713

Staudt, G. (1982). Pollen germination and pollen tube growth in vivo and the dependence on temperature. *Vitis* 21, 205-216.

Storkey, D. et al. (2018). UK Global Ocean GO6 and GO7: a traceable hierarchy of model resolutions *Geosci. Model Dev.* 11 3187–213 https://doi.org/10.5194/gmd-11-3187-2018

Sutton, P. J.H., Bowen, M & Roemmich, D. (2005) Decadal Temperature changes in the Tasman Sea. *New Zealand Journal of Marine and Freshwater Research* 39(6), 1321–1329 https://doi.org/10.1080/00288330.2005.9517396

Simmonds, I., and K. Keay, 2000: Mean Southern Hemisphere extratropical cyclone behaviour in the 40-year NCEP–NCAR reanalysis. *J. Climate* 13, 873–885 https://doi.org/10.1175/1520-0442(2000)013<0873:MSHECB>2.0.CO;2

Trenberth, K.E. 1976. Fluctuations and trends in indices of the southern hemispheric circulation. *Quarterly Journal of the Royal Meteorological Society* 102(431), 65-75 https://doi.org/10.1002/qj.4971024310

751 Trenberth, K.E. 1984. Signal versus noise in the Southern Oscillation. *Mon. Wea. Rev.* 112, 326-
752 332. https://doi.org/10.1175/1520-0493(1984)112<0326:SVNITS>2.0.CO;2
753 Trenberth, K. E., (1991). Storm tracks in the southern hemisphere. *J. Atmos. Sci*., 48, 2159–2178.
754 http://dx.doi.org/10.1175/1520-0469(1991)048<2159:STITSH>2.0.CO;2
755 Trenberth, K. E., G. W. Branstator, D. Karoly, A. Kumar, N-C. Lau, and C. Ropelewski, 1998:
756 Progress during TOGA in understanding and modeling global teleconnections associated with
757 tropical sea surface temperatures. *Journal Geophysical Research*, 103**,** 14291–14324.
758 http://dx.doi.org/10.1029/97JC01444
759 Trenberth, K. E., P. D. Jones, P. Ambenje, et al. 2007: *Observations: Surface and Atmospheric*
760 *Climate Change.* In: *Climate Change 2007. The Physical Science Basis*. Fourth Assessment
761 Report of the Intergovernmental Panel on Climate Change. [S. Solomon, D. Qin, M.
762 Manning, et al. (eds)]. Cambridge University Press, 235–336.
763 Trenberth, K.E, Y. Zhang, J.T.Fasullo and L.Cheng (2019) Observation-Based Estimates of Global
764 and Basin Ocean Meridional Heat Transport Time Series. *Journal of Climate 32,* 4567-
765 4583 https://doi.org/10.1175/JCLI-D-18-0872.1
766 Trought, M.C.T. 2005. Fruitset - possible implications on wine quality. In: *Transforming flowers to*
767 *fruit. Mildura, Australia: Australian Society of Viticulture and Oenology*, edited by Garis, K.
768 D., Dundon, C., Johnstone, R. & Partridge, S., Australian Society of Viticulture and
769 Oenology, Mildura, Australia: 32-36.
770 Tsujino, H., et al. 2018. JRA-55 based surface dataset for driving ocean–sea-ice models (JRA55-do).
771 *Ocean Modelling*, 130 (October 2018), 79-14. https://doi.org/10.1016/j.ocemod.2018.07.002
772 Vargo, L. J., Anderson, B. M., Dadić, R., Horgan, H. J., Mackintosh, A. N., King, A. D. & Lorrey, A.
773 M. (2020). Anthropogenic warming forces extreme annual glacier mass loss. *Nature Climate*
774 *Change*, 10(9), 856-861. https://doi.org/10.1038/s41558-020-0849-2

775 Willsman, A., & Macara, G. (2023) New Zealand Glacier Monitoring: End of summer snowline
776 survey 2021. Report prepared for Ministry of Business, Innovation and Employment. 157 pp.
777 Zhu, J.; Fraysse, R.; Trought, M.C.T.; Raw, V.; Yang, L.; Greven, M.; Martin, D.; Agnew, R**.** (2020)
778 Quantifying the seasonal variations in grapevine yield components based on pre- and post-
779 flowering weather conditions. *Oeno One* 54 (2), 213-230, DOI:
780 https://doi.org/10.20870/oeno-one.2020.54.2.2926.
781 Zscheischler, J., Westra, S., van den Hurk, B.J.J.M. *et al.* 2018. Future climate risk from compound
782 events. *Nature Clim Change* 8, 469–477 (2018). https://doi.org/10.1038/s41558-018-0156-3
783 Zuo, H., Balmaseda, M. A., Tietsche, S., Mogensen, K., and Mayer, M.: The ECMWF operational
784 ensemble reanalysis–analysis system for ocean and sea ice: a description of the system and
785 assessment, Ocean Sci., 15, 779–808, https://doi.org/10.5194/os-15-779-2019, 2019.

Metric	1934/35	2017/18	2018/19	2021/22	2022/23
NZ22T	**+1.30**	**+1.62**	**+1.07**	**+1.11**	+0.85
NZERSSTv5	**+0.64**	**+1.06**	**+0.84**	**+0.83**	**+0.91**
NZEEZ	**+0.70**	**+1.13**	**+0.87**	**+0.81**	**+0.94**
SAM	**+1.45**	**+1.67**	**+0.98**	**+2.16**	**+1.63**
NINO3.4	+0.10	-0.90	+0.79	-0.97	-0.56
SOI	**+0.66**	**+0.56**	-0.72	**+2.16**	**+2.36**
IPO	-0.021	**-0.925**	0.146	**-1.328**	**-1.00**
Z1	**-23**	**-17**	-11	**-33**	**-31**
M1	**-52**	**-27**	**-35**	-3	**-80**
Trough	NA	-6.7	**+7.7**	**-10.7**	**+**1.7
Zonal	NA	**-15.5**	-3.8	**-15.1**	**-15.7**
Block	NA	**22.6**	+6.4	**+26.0**	+5.3
Warm days TX90p	**26**	**33**	**22**	**19**	**17**
Days ≥25ºC	**22**	**32**	**26**	**31**	**21**

Table 1. Indices for the five heatwaves for NDJFM. NZ22T is the 22 station NZT series for surface temperature over the land area of NZ, NZERSST is the ERSST version 5 for the NZ Zealand (NZ) EEZ and ECS, 34 to 48°S, and 165° to 179°E, and NZEEZT are NZ22T and NZERSST combined and weighted for the entire NZ region with anomalies in °C. All temperature departures are anomalies from the 1991-2020 climatology period for the months of November – March. NZ22T mean 0.02 °C, standard deviation (s.d.) of ±0.42°C, NZERSST mean 0.0, s.d ±0.29°C, and NZEEZT mean -0.2 s.d ±0.54 °C.

The Southern Annular Mode (SAM) (Fogt et al. 2009) mean 0.06, s.d 1.08, Nino3.4 the Index mean 0.0, s.d 1.3, the Climate Analysis Section NCAR Southern Oscillation Index (SOI, Trenberth 1984) mean 0.0, s.d. 1.0 and the Interdecadal Pacific Oscillation (IPO) the tripolar index (Henley et al. 2015) mean -0.9, s.d. 0.83, Z1 (mean +0.3 s.d. 14.5) and M1 (mean +1.2, s.d, 19.6) are Trenberth (1976) zonal and meridional indices. Kidson regimes are Trough, Zonal and Block anomalies (Kidson 2000). TX90p is the percentage of days above the daily maximum (TX) (mean is 10% 1951-1980 climatology period), with Days > 25ºC counts, all averaged for 26 NZ climate stations. Mean counts days > 25ºC 15.0, d +/- 5.2 days. Bolded values significant at $p<0.05$.

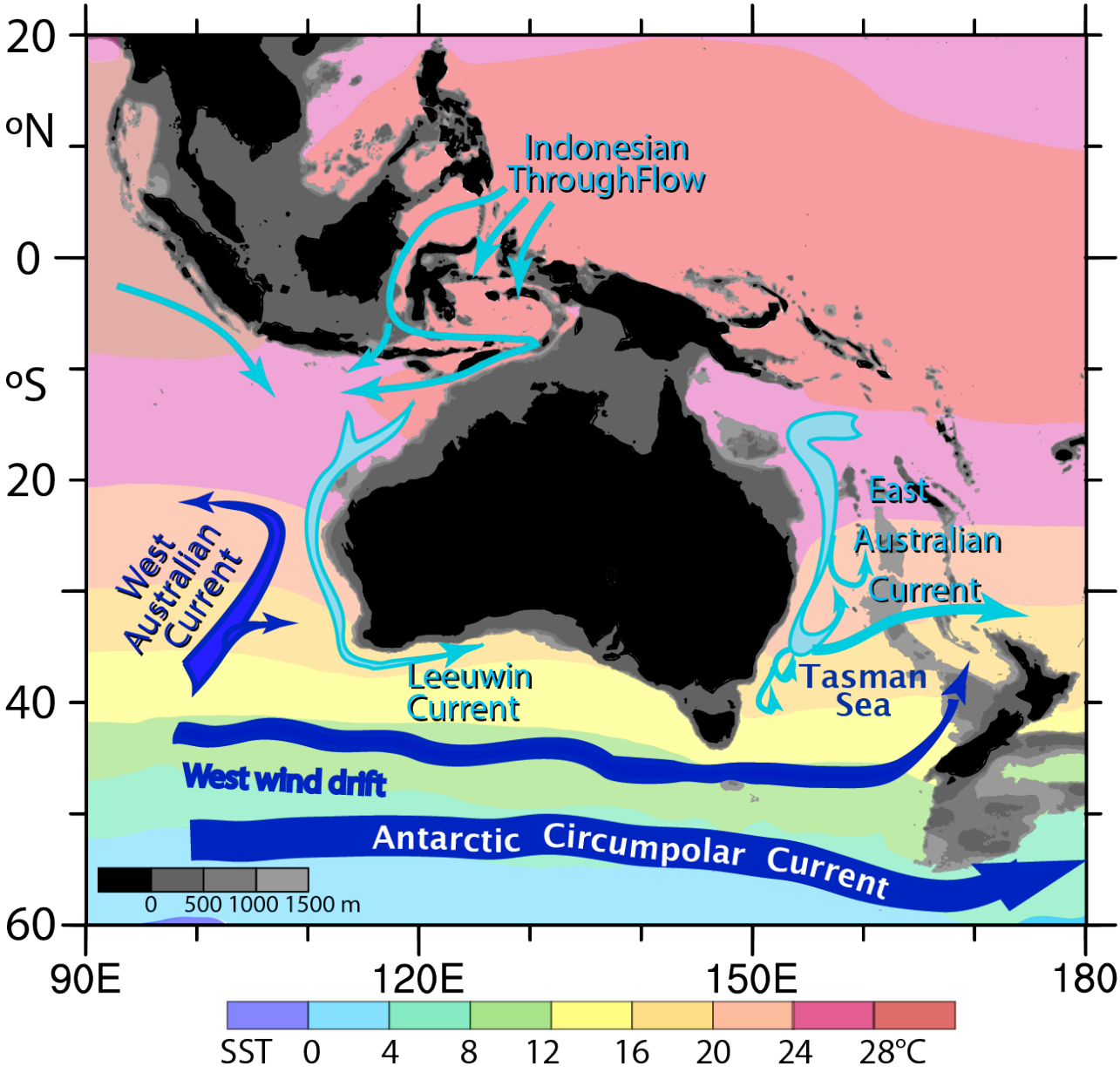

Figure 1. The shades of grey show bathymetry at the surface (black), 500, 1000, and 1500 m depth. The background field is the annual mean SST, scale at bottom. The arrows depict various currents; the cyan arrows show warm waters in the ITF, East Australian current or Leeuwin current. The dark blue s arrows show the Antarctic Circumpolar Current and the associated West-wind drift, plus the West Australian current. The Tasman Sea lies between Australia and New Zealand (NZ). From Trenberth and Zhang (2019).

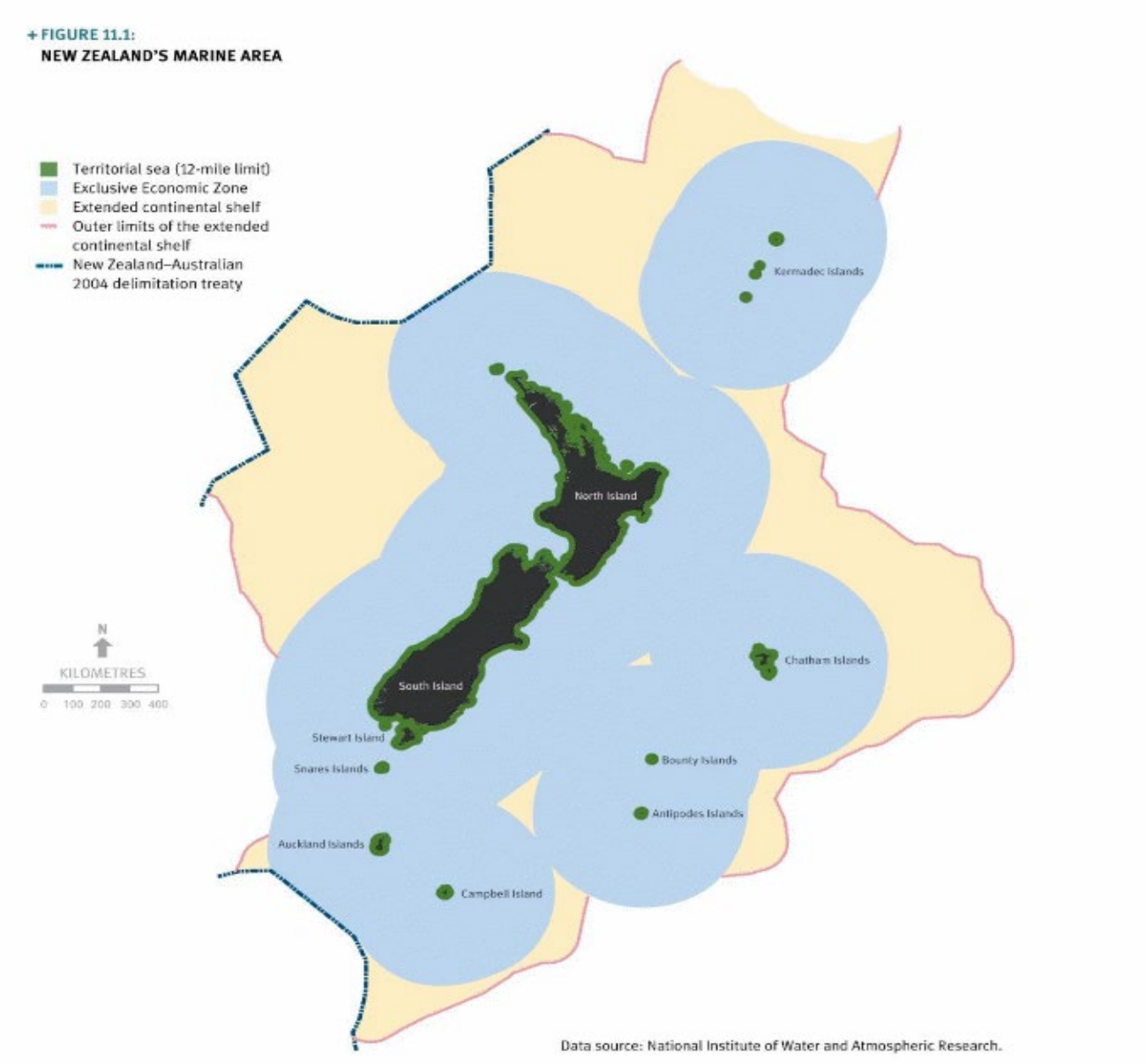

Figure 2. New Zealand's marine area, showing the territorial sea (green), EEZ (Blue) and extended continental shelf (orange). (Source: NIWA Risk Assessment).

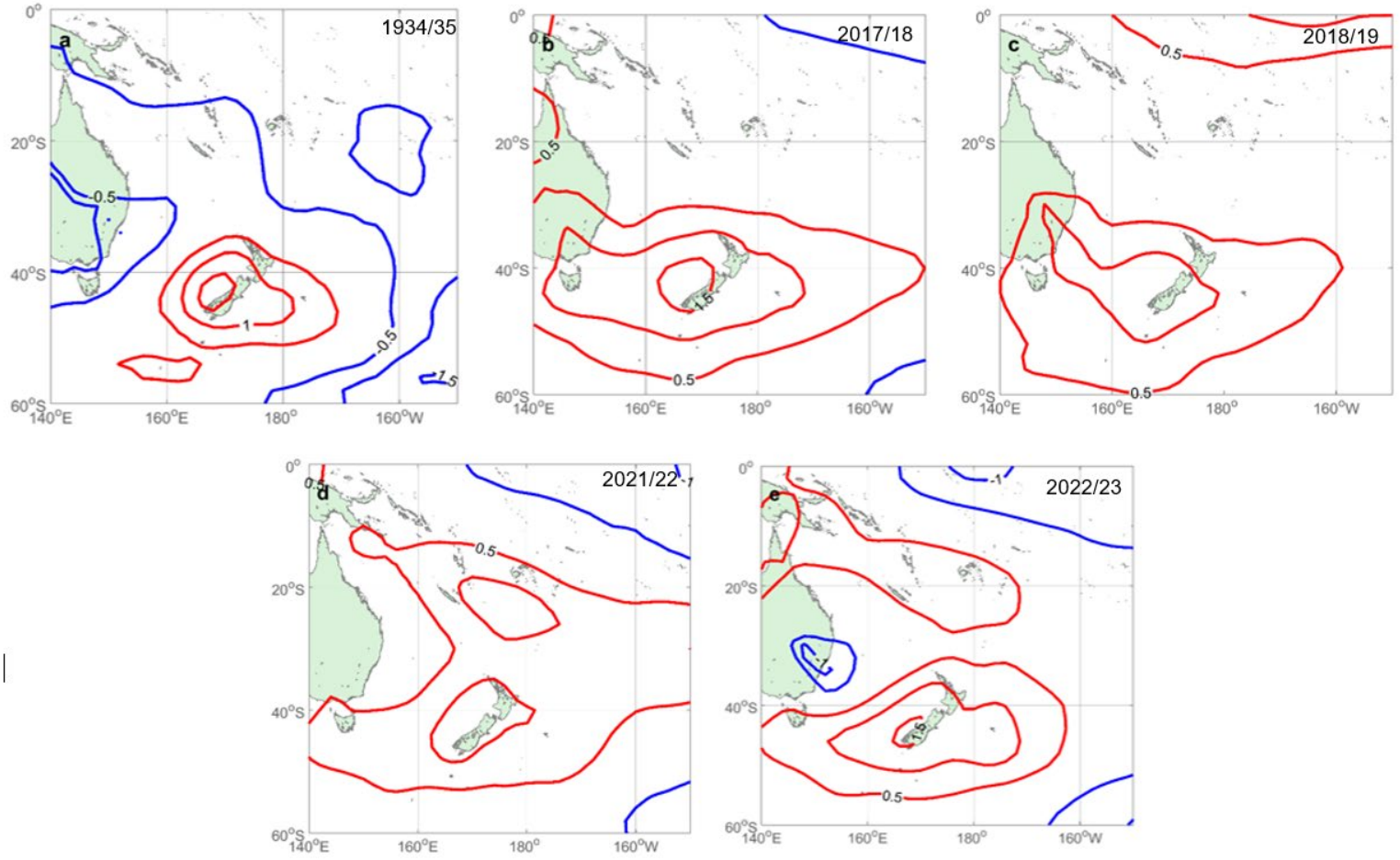

Figure 3. ERSSTv5 (Huang et al 2017) SST anomalies (0.5ºC contours) for the Tasman Sea/New Zealand for the 5 most intense Austral warm season (NDJFM) AHW/MHW heatwaves using the 1991-2020 climate base period. (a) 1934/35, (b) 2017/18, (c) 2018/19, (d) 2021/22, and (e) 2022/23. In all cases, negative contours are blue, positive are red, and the zero contour has been suppressed. See Table 1 for index values.

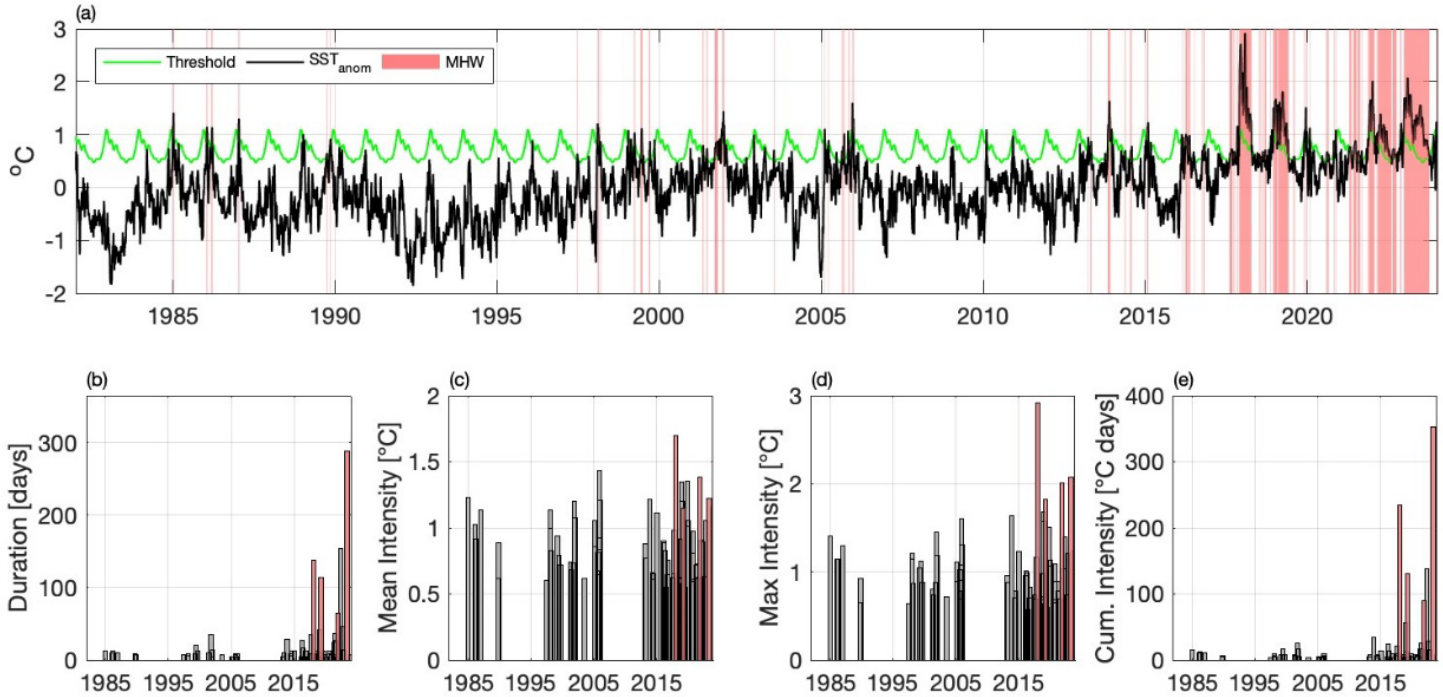

843

844 **Figure 4.** (a) Time series of area-averaged sea surface temperature (SST) anomalies January 1982 to December 2023 SSTs (black) with MHW
845 threshold (green), base climatology (1991-2020), for coastal waters (out to 12 nautical miles offshore) of NZ 90th percentile. The red shaded
846 regions identify periods associated with MHWs using the Hobday et al. (2016) definition. Also shown are the (b) duration, (c) mean intensity, (d)
847 maximum intensity and (e) cumulative intensity of each MHW detected in the area-averaged SST time series, with the four individual MHWs
848 with the highest maximum intensity detected in the time series highlighted by red shading.

849

850

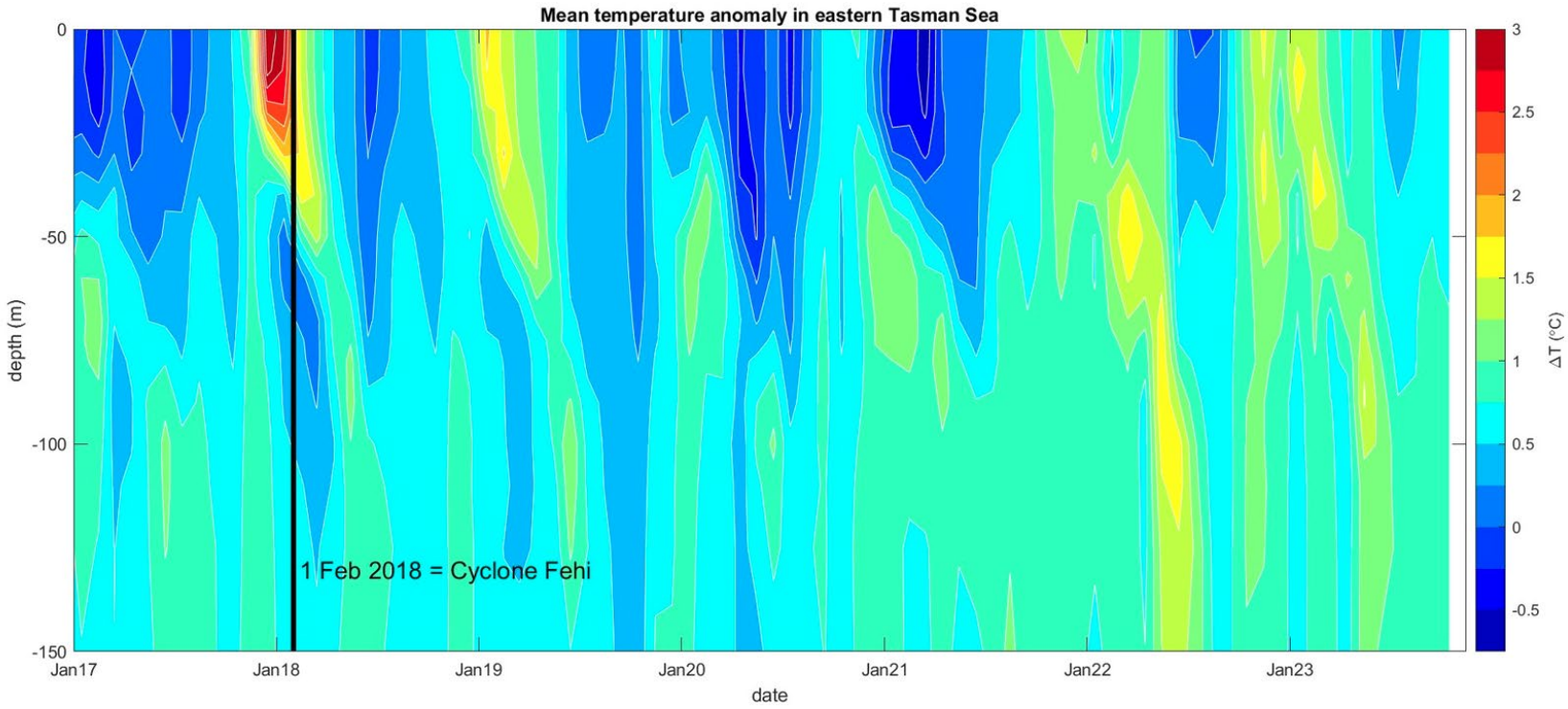

851

852 **Figure 5**. Monthly subsurface temperature anomalies in the eastern Tasman Sea (162 – 172° E, 35 - 45°S) from Argo floats January 2017 – May

853 2023.

854

855

856

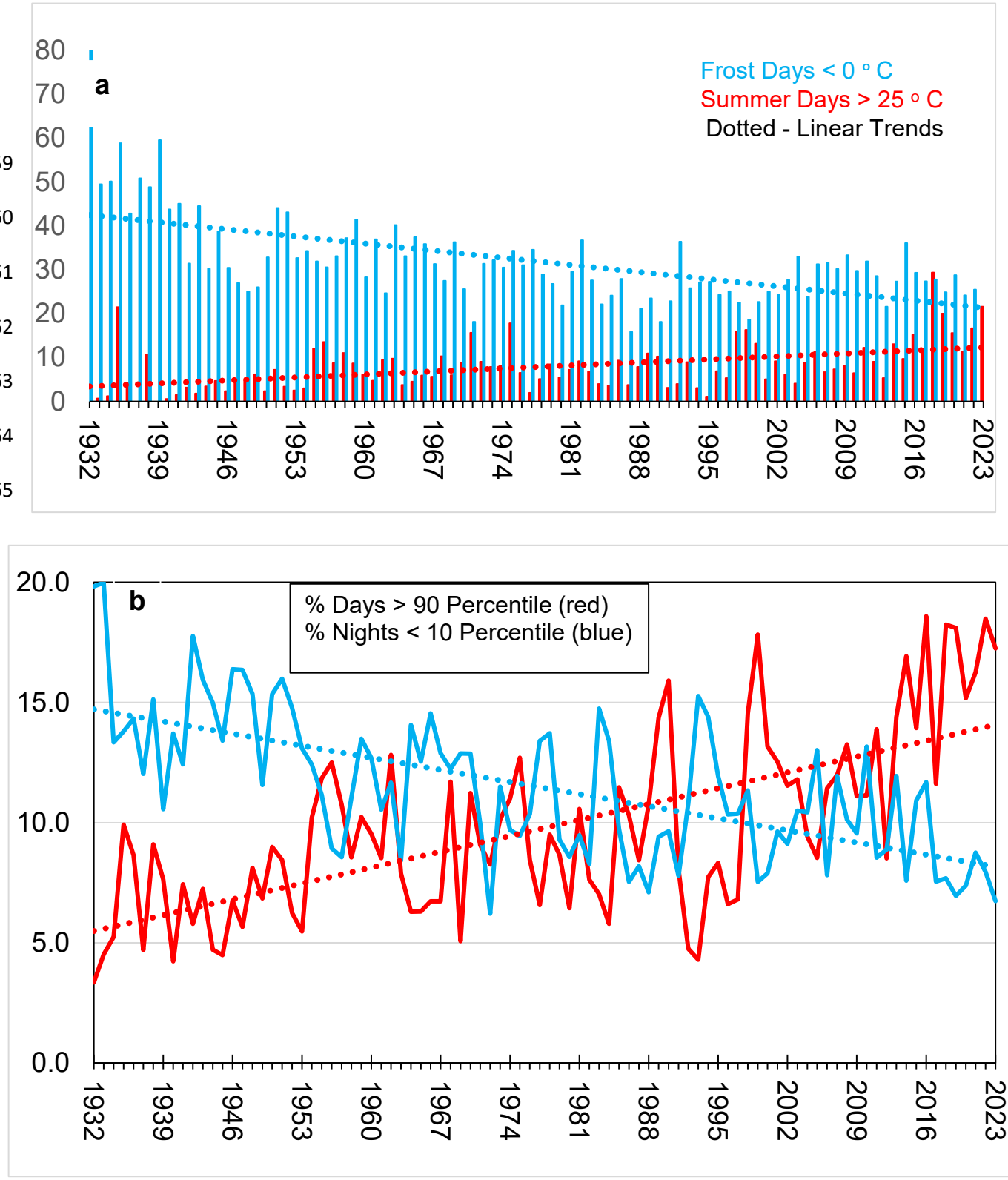

Fig. 6. Warm and cold extremes 1931-2023. (a). Summer days >25ºC (July – June) (red bars) and frost days < 0ºC (January - December) (blue bars) and trends (dotted) for NZ land climate stations, and (b) annual TX90p and TN10p, percentages of days above the maximum (TX) and minimum (TN) daily 10 percentile (mean is 10% 1991-2020 climatology period) and trends (dotted) land stations.

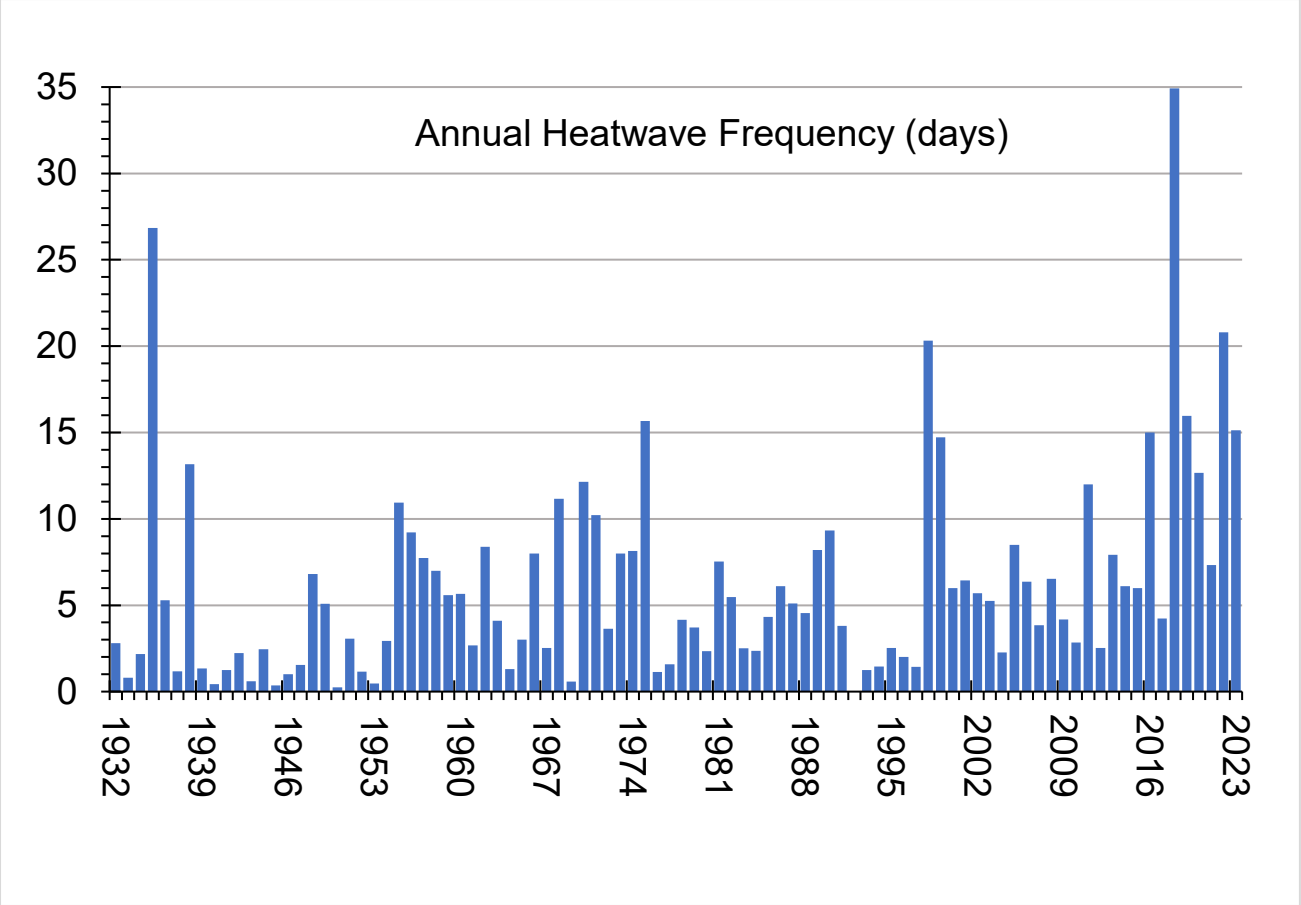

871

872 **Fig. 7. Annual frequency of heatwave days (HWF).** HWF is defined as 3 or more days

873

874

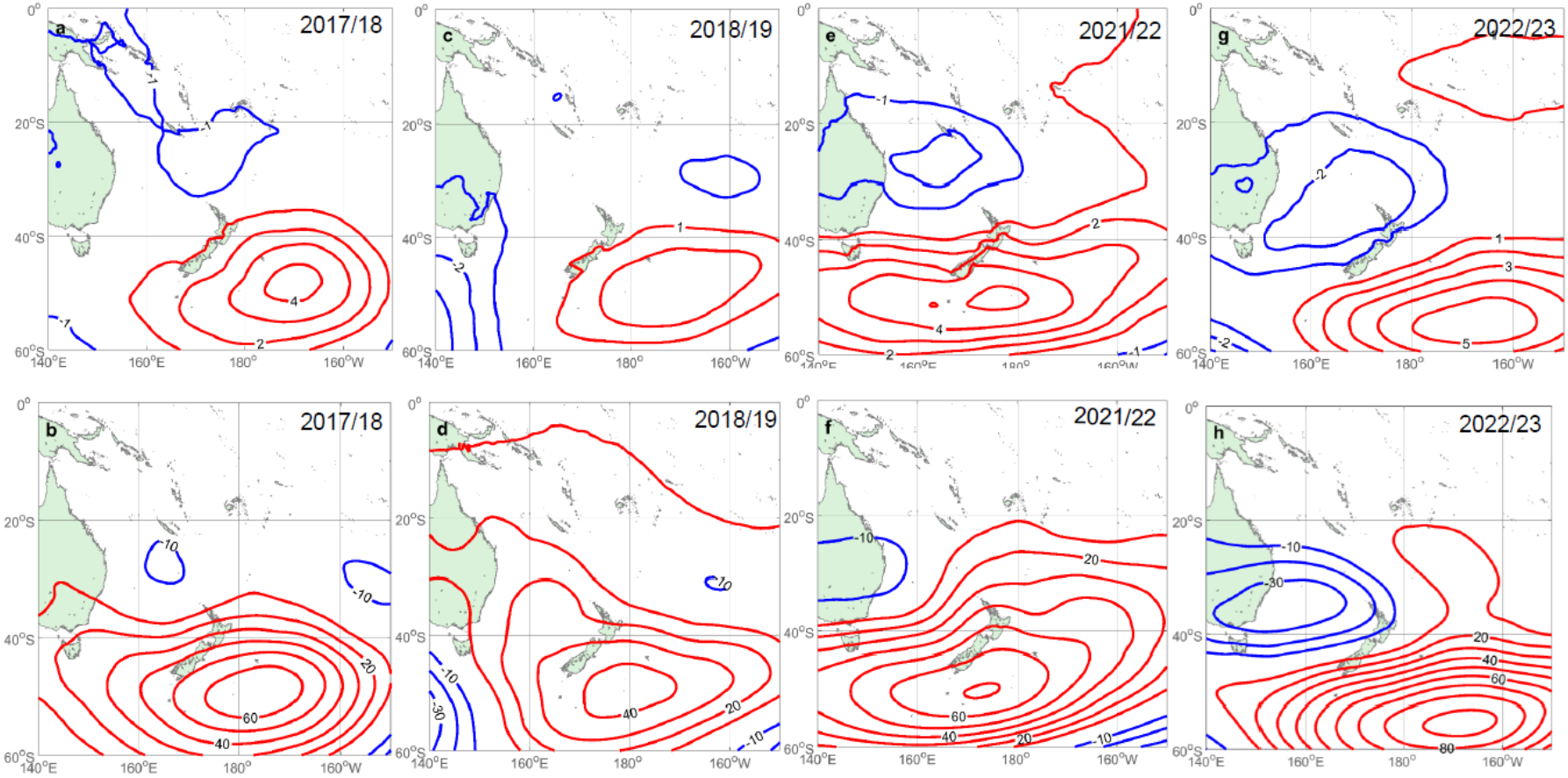

875

876 **Figure 8.** Atmospheric circulation anomaly patterns using ERA-5 Reanalysis (Bell et al 2021) with 1991-2020 base period. NDJFM mean sea

877 level pressure anomaly (1 hPa contours): a. 2017/18, c. 2018/19, e. 2021/22, and g. 2022/23. NDJFM 500-hPa Geopotential Height anomaly (10

878 gpm contours): b. 2017/18, d. 2018/19, f. 2021/22, and h. 2022/23. In all cases, negative contours are blue, positive are red, and the zero contour

879 has been suppressed. See Table 1 for index values.

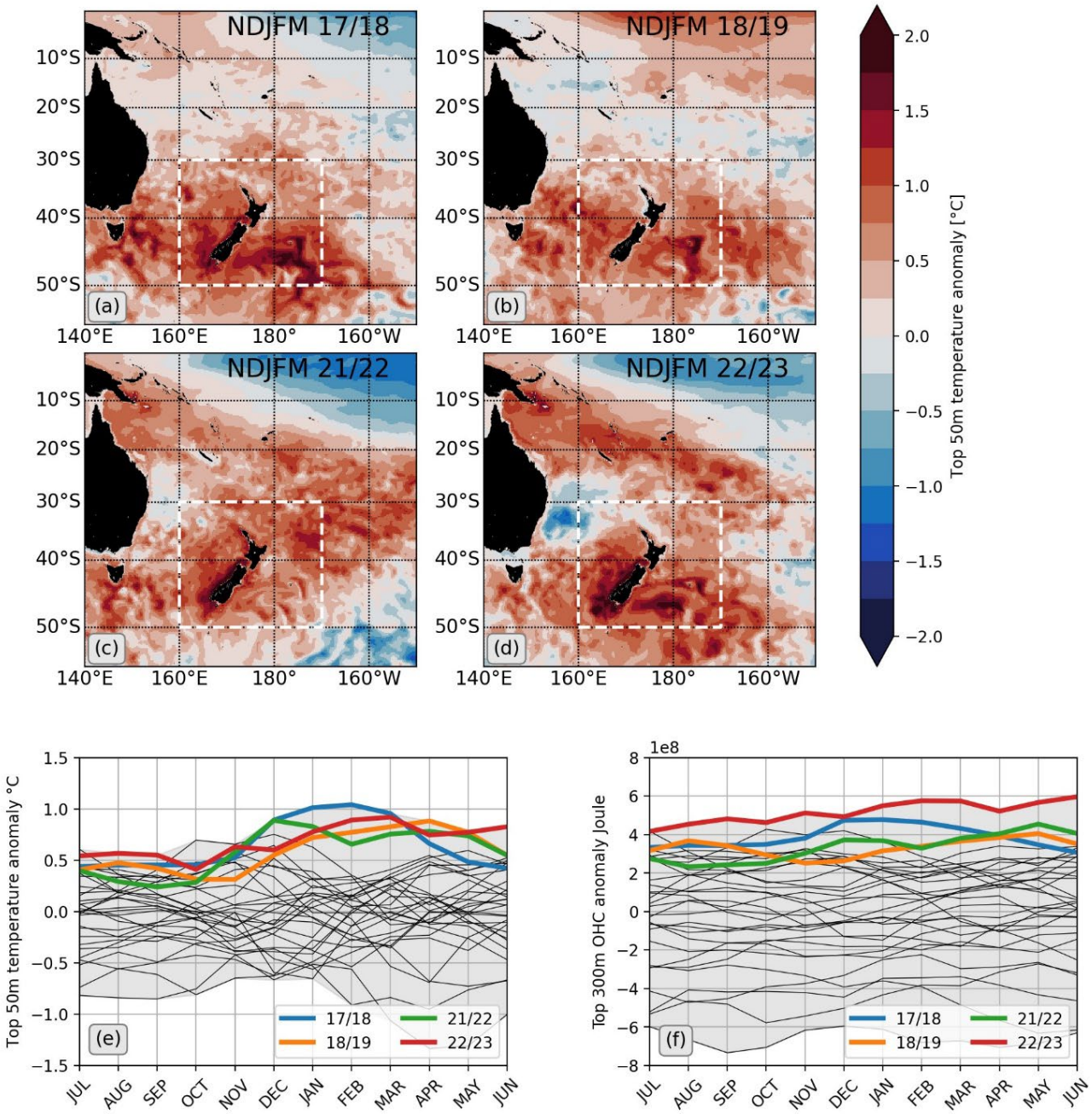

Figure 9. Modelled top 50m temperature anomalies relative to the climatological mean over the period 1991-2023. (a) November-March 2018/19, (b) November - March 2019-2020, (c) November - March 2021/22 and (d) November - March 2022/23. (e) Top 50m area-averaged temperature anomalies over the region 160°E-170°W and 50°S-30°S (white dashed box in a-d) for individual years from 1991-2023 (black lines) with the four warmest summers (a-d) colour coded, (f) Sames as (e) but for top 300m OHC anomalies, with the four warmest summers (a-d) colour coded.

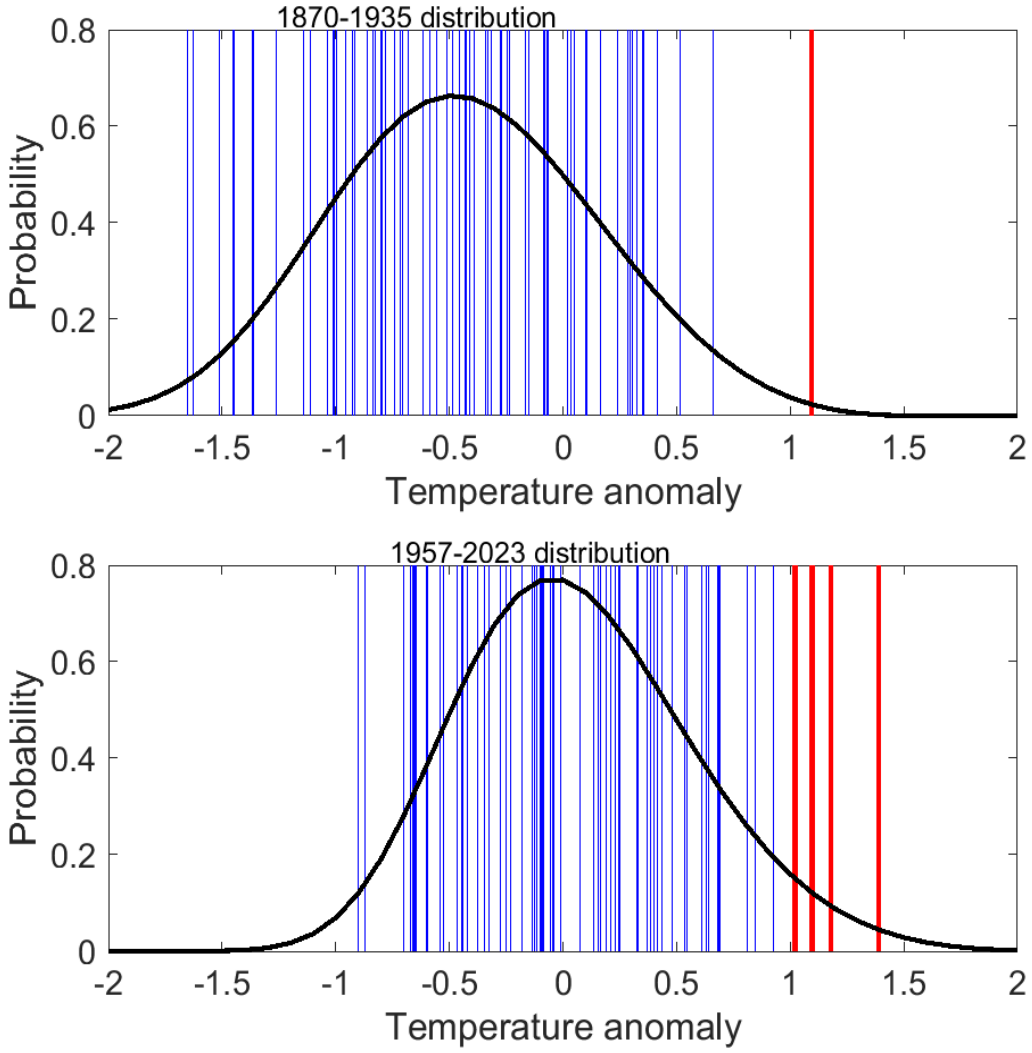

902

903 **Figure 10.** Probability distributions of warm season periods (November – March) for the period up
904 to the extreme occurrences. (a) 1870 – 1935, and (b) 1957 – 2023. Heatwave seasons marked in red
905 (see Table 1) and all other seasons in blue. The black lines show fitted GEV distributions.

906

907

908

909

910

911

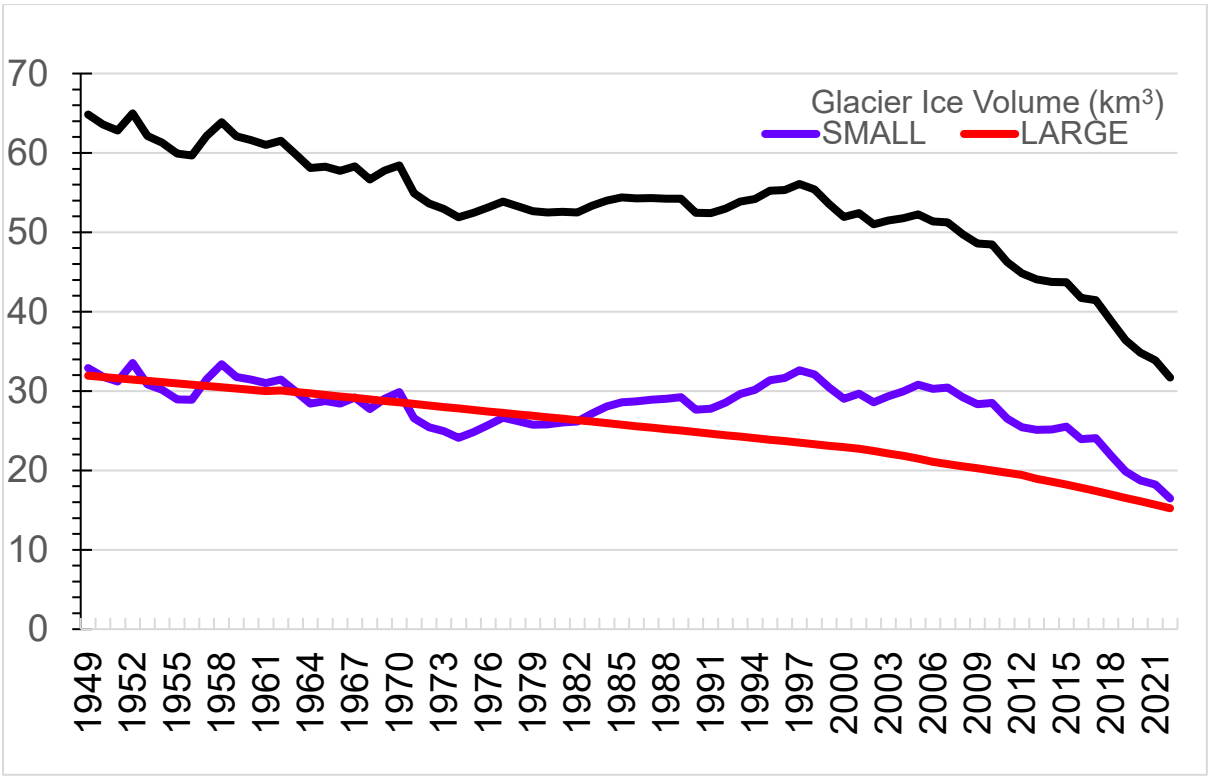

912

913 **Figure 11**. Southern Alps Ice volume km^3, total for all (black), large (red) and small (blue) glaciers.

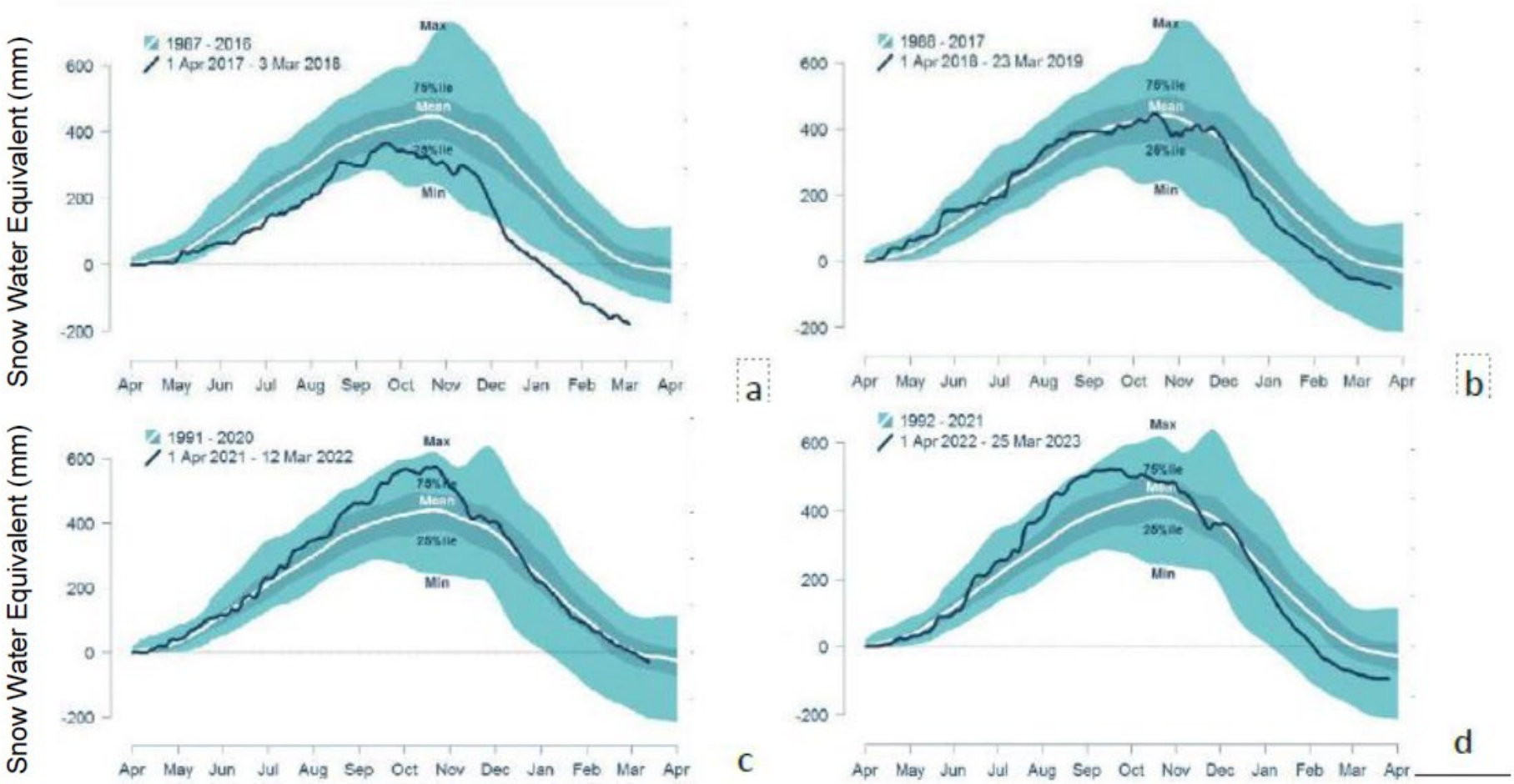

- **Figure 12. a - d.** Estimated water stored as seasonal snow, in snow water equivalents (SWE) (mm), for the Waikati catchment, South Island, from SnowSim for the AHW years. (a) 2017/18, (b) 2018/19, (c) 2021/22 and (d) 2022/23. The white curve is the mean SWE for the periods indicated, with the maximum, 75 and 25 percentiles and minimum SWE indicated.

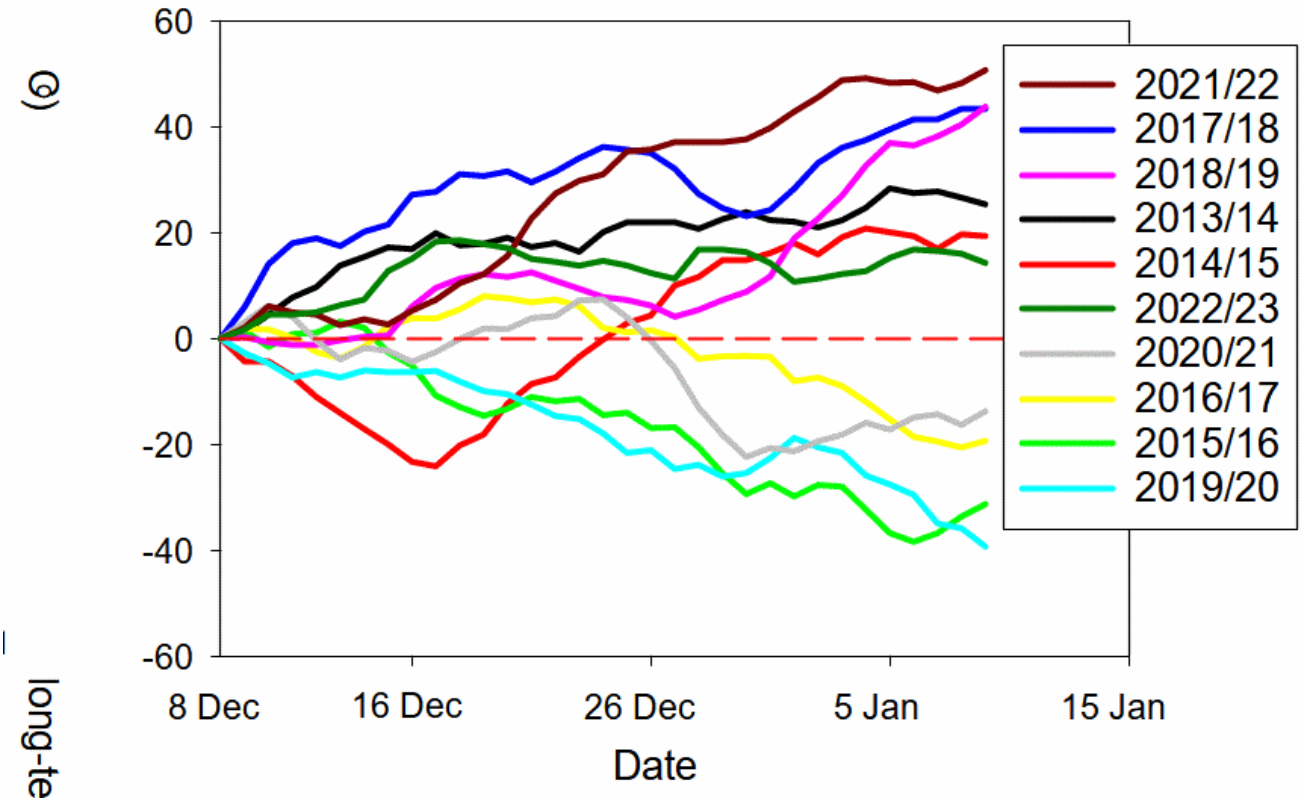

Figure 13. Seasonal changes. Seasonal deviation in accumulated mean daily temperature from the start to end of flowering (veraison) of Marlborough Sauvignon blanc grapes for ten growing seasons 2013/14 to 2022/23.